의학박사 학위논문

글리칸 부적합 장기이식에서 글리칸 항원에 대한 체액성 면역반응의 조절

Regulation of humoral immunity against glycan antigens in glycan-incompatible transplantation

2017년 8월

서울대학교 대학원

의학과 중개의학(면역학)

허 성 훈

글리칸 부적합 장기이식에서 글리칸 항원에 대한 체액성 면역반응의 조절

지도교수 안 규 리

이 논문을 의학박사 학위논문으로 제출함

2017년 4월

서울대학교 대학원

의학과 중개의학(면역학)

허 성 훈

허성훈의 박사학위논문을 인준함

2017년 6월

위 원 장 하 일 수 (인)

부 위 원 장 안 규 리 (인)

위 원 채 동 민 (인)

위 원 정 준 호 (인)

위 원 황 종 익 (인)

Regulation of humoral immunity against glycan antigens in glycan-incompatible transplantation

by

Sunghoon Hurh

A thesis submitted to the Department of Medicine in partial fulfillment of the requirements for the Degree of Doctor of Philosophy in Translational Medicine (Immunology) at Seoul National University College of Medicine

June 2017

Approved by Thesis Committee:

Professor _____ Chairman

Professor _____ Vice chairman

Professor _____

Professor _____

Professor _____

Abstract

Regulation of humoral immunity against glycan antigens in glycan-incompatible transplantation

Sunghoon Hurh

Major in Translational Medicine, Department of Medicine

The Graduate School

Seoul National University

Although clinical transplantation is the most effective therapy for patients with end-stage organ failure, this treatment has a limitation caused by the severe shortage of organ resources. Glycan-incompatible transplantation such as ABO-incompatible (ABOi) allotransplantation and xenotransplantation using pig organs has been considered as one of solutions to alleviate the limitation. However, there are a number of problems that need to be overcome for glycan-incompatible transplantation to be successful, in particular antibody-mediated responses toward glycan antigens on donor endothelium.

Firstly, owing to the molecular incompatibility between human and pig, a slight binding of human antibody to pig endothelium can activate complement

and coagulation system. To overcome a series of transplant rejections caused by molecular incompatibility, transgenic pigs expressing multiple human genes are required. The generation of multiple transgenic pigs either by breeding or the introduction of several mono-cistronic vectors has been hampered by the differential expression patterns of the target genes. To achieve simultaneous expression of multiple genes, a poly-cistronic expression system using the 2A peptide derived from the Thosea asigna virus (T2A) was adopted. To evaluate the effect of T2A expression system, I constructed several bi-cistronic T2A expression vectors, which combine target genes that are frequently used in the xenotransplantation field, and analyzed the expression pattern of target genes using porcine fibroblasts. The proteins targeted to the same or different subcellular regions were efficiently expressed without affecting the localization or expression levels of the other protein and the adequate expression of downstream genes can be achieved if the expression of the upstream gene is efficient. Therefore, T2A expression system is a promising tool for generating transgenic pigs that express multiple target genes for xenotransplantation.

Secondly, humoral immune responses caused by preformed antibodies against pig glycan antigens are critical hurdles that need to be overcome. Despite the development of α1,3-galactosyl transferase-knockout (GT-KO) pigs, acute humoral xenograft rejection caused by antibodies against non-Gal antigens have been observed. Among non-Gal antigens, *N*-glycolylneuraminic acid (Neu5Gc) is considered to play an important role in xenograft rejection in human. To study human preformed antibody responses to Neu5Gc, I generated human embryonic

kidney 293 (HEK293) cells that expressed xenogeneic Neu5Gc (HEK293-pCMAH) or α1,3Gal (HEK293-pGT) antigen and investigated the degree of human antibody binding and complement-dependent cytotoxicity (CDC) against these antigens using 100 individual human sera. Both IgM and IgG bound to α1,3Gal, while only IgG bound to Neu5Gc. Although the antibody reactivity to Neu5Gc was highly variable among individuals, severe CDC was significantly observed in HEK293-pCMAH responded with some human sera. In addition, the severity of CDC against HEK293-pCMAH cells positively correlated with that against GT-KO pig aortic endothelial cells (PAECs), suggesting that Neu5Gc is the main antigen in GT-KO PAECs. These results suggest that additional modifications to the CMAH gene will be required for widespread use of pig organs for human transplants.

Thirdly, even though hyperacute rejection (HAR) can be prevented by using antibody desensitization protocols and GT-KO pigs, acute and chronic antibody mediated rejection induced by de novo synthesized antibodies after transplantation can be an another hurdle. For glycan-incompatible transplantation situation, it is unknown that which B cell subsets can recognize certain carbohydrate antigens, whether the responses are T cell dependent or independent, and whether T cells can recognize the certain carbohydrate antigens in antigen presenting molecules. To solve the questions, I established mice model for investigating induced anti-carbohydrate antibody production using target carbohydrate antigen-deficient mice and representative cell lines expressing target carbohydrate antigens, α1,3Gal, Neu5Gc, or blood group A, respectively. The

induced antibodies against each carbohydrate antigens (α1,3Gal, Neu5Gc, or blood group A) are specific to target antigen. The mechanism of induced antibodies production against each carbohydrate antigen was quite different from each other. Interestingly, $CD4^+$ T cell depletion effectively inhibited the production of induced antibody against three carbohydrate antigens altogether in mice. However, further study will be required to confirm whether the regulation of $CD4^+$ T cell can ameliorate induced antibody responses in non-human primate and human.

Keywords: glycan antigen, preformed antibody, induced antibody, humoral immune response, ABO-incompatible transplantation, xenotransplantation, polycistronic expression system

Student Number: 2011-31149

Contents

List of tables

Chapter I

List of figures

Chapter I

Chapter II

Chapter III

List of abbreviations

7-AAD	7-Aminoactinomycin D
ABOi	ABO-incompatible
AF647	Alexa Fluor 647
AHXR	acute humoral xenograft rejection
ANOVA	Analysis of variance
APC	allophycocyanin
APCs	antigen presenting cells
A-RBC	red blood cell expressing bloog group A
B6	C57BL/6 mouse
B6.ATg	B6-huHAT(ICAM) transgenic (Tg) mouse
BCR	B cell receptor
BSA	bovine serum albumin
BS-IB4	Bandeiraea simplicifolia isolectin B4
C2D	MHC class II-deficient
C4a	complement component 4a
CAG promoter	chicken β-actin promoter
CDC	complement-dependent cytotoxicity
cDNA	complementary DNA
CMAH	cytidine monophosphate-N-acetylneuraminic acid hydroxylase
CMV	cytomegalo virus
DMEM	Dulbecco's modified Eagle medium
E2A	2A peptide from the Equine rhinitis A virus

EGFP	enhanced green fluorescent protein
ER	endoplasmic reticulum
F2A	2A peptide from FMDV
FBS	fetal bovine serum
FITC	fluorescein isothiocyanate
FMDV	foot and mouth disease virus
gDNA	genomic DNA
GDS	IgG-depleted serum
GT-KO	α1,3-galactosyl transferase-knockout
HA	hemaglutinin
HAR	hyperacute rejection
hAT	human A-transferase
hCD39	human CD39
hCD46	human CD46
hCD55	human CD55
hCD59	human CD59
HEK293	human embryonic kidney 293
HEK293-ATg	HEK293 cells stably expressing hHT and hAT
HEK293-pCMAH	HEK293 cells stably expressing the pCMAH
HEK293-pGT	HEK293 cells stably expressing the pGT
hHO1	human heme oxygenase 1
hHT	human H-transferase
HIS	heat-inactivated serum

HRP	horseradish peroxidase
hTBM	human thrombomodulin
IACUC	Institutional Animal Care and Use Committee
iNKT	invariant natural killer T
iPSC	induced pluripotent stem cell
IRB	Institutional Review Board
IRES	internal ribosome entry site
IRES-Ex	IRES expression
ITAF	IRES trans-acting factors
MFI	mean fluorescent intensity
MHC	major histocompatibility complex
miRNA	microRNA
MPN3	WT pig aortic endothelial cell line
MPN3-ATg	MPN3 cells stably expressing hHT and hAT
mRNA	messenger RNA
MS1	MILE SVEN 1 cell (B6 mouse vascular endothelial cell line)
MS1-ATg	MS1 cells stably expressing hHT and hAT
MZB cell	marginal zone B cell
Neu5Ac	N-acetylneuraminic acid
Neu5Gc	N-glycolylneuraminic acid
NTHi	nontypeable Haemophilus influenzae
OD	optical density
P2A	2A peptide from the Porcine teschovirus-1

PAA	Polyacrylamide
PAEC	pig aortic endothelial cell
PBMC	peripheral blood mononuclear cell
PBS	phosphate-buffered saline
PCR	polymerase chain reaction
PE	phycoerythrin
PerCP	Peridinin-Chlorophyll protein
RT	room temperature
RT-PCR	reverse transcription polymerase chain reaction
SD	standard deviations
siGFP	GFP-targeted siRNA
siLuc	Luciferase-targeted siRNA
siRNA	small interfering RNA
SST	serum separation tube
SV40T	SV40 large T antigen
T2A	2A peptide from the Thosea asigna virus
T2A-Ex	T2A expression
TBE	Tris/Borate/EDTA
TBS	Tris-buffered saline
TBST	Tris-buffered saline containing Tween-20
TCRβ	T cell receptor β chain
TLR	Toll-like receptor
Traj	T cell receptor alpha joining

UTR	untranslated region
WT	wild-type
α1,3Gal	galactose-α-1,3-galactose antigen

Chapter I

Development of polycistronic expression system for multi-transgenic pigs

Reprinted or edited from

PLoS One. 2013;8(7):e70486.

Introduction

Due to the severe shortage of human donor tissues and organs, xenotransplantation has been considered as a potential alternative to allotransplantation. However, the clinical application of pig-to-primate xenotransplantation has been hampered by a series of obstacles, including hyperacute rejection (HAR), acute humoral xenograft rejection (AHXR), and cellular rejection [1]. Because of these complex and robust immune responses, it has become clear that the modulation of one or two target genes is insufficient for successful xenotransplantation. For example, the kidneys from α1,3-galactosyl transferase-knockout (GT-KO)/human CD46 (hCD46) transgenic pigs that were transplanted into baboons were rejected within 16 days [2], and the kidneys from GT-KO pigs transgenic for human CD55 (hCD55), hCD59, hCD39, and H-transferase (hHT) that were transplanted into baboons were rejected by AHXR within 15 days [3]. Thus, the generation of transgenic pigs that stably express multiple immune-modulating molecules is essential for overcoming xenograft rejection.

Multiple transgenic pigs have generally been produced by breeding [4] or via the transfection of multiple mono-cistronic plasmids containing target genes [5, 6]. However, breeding is time-consuming and expensive, and the target gene expression levels frequently decrease over time. Pigs generated by multiple plasmid transfections exhibit poorly synchronized expression of target genes. The alternative approach for generating multiple transgenic pigs is the use of a poly-cistronic expression system containing an internal ribosome entry site (IRES) or a viral 2A peptide. Various IRESs derived from viral genomes or eukaryotic

messenger RNAs (mRNAs) have been widely distributed [7]. However, one of the major problems with the use of an IRES system is that the IRES-dependent expression of the second gene is significantly reduced compared with that of the first cap-dependent gene in mammalian cells [8, 9]. Furthermore, the translation efficiency was highly variable depending upon the origin of IRES or the transduced cell types [10, 11] because each IRES requires different IRES trans-acting factors (ITAFs) [12, 13].

Viral 2A peptides were initially identified in the viruses of the picornaviridae family, such as foot and mouth disease virus (FMDV) and cardiovirus. 2A peptides are composed of approximately 19 amino acids, including the consensus motif D(V/I)EXNPGP. “Self-cleaving” occurs through a ribosomal skipping mechanism, which might inhibit the formation of a peptide bond between the glycine and proline residues within the consensus motif [14]. When a 2A peptide exists between two genes, after the translation of the upstream gene, the ribosome skips translation at the glycine-proline junction in the 2A peptide and continues to translate the downstream gene. Previous studies have shown that the efficiency of this ribosomal skip is highly variable, depending on the sequences in upstream region of the consensus motif in the 2A peptides [15]. The efficiencies of the ribosomal skip were not equal among representative 2A peptides [16], such as the F2A peptide from FMDV, E2A from the Equine rhinitis A virus, P2A from the Porcine teschovirus-1, and T2A from the Thosea asigna virus [17-19]. Therefore, the selection of an optimal 2A peptide is determinant for the stable expression of target genes. Donnelly et al. previously tested several 2A peptides from different viral genes and showed that the T2A peptide exhibited favorable cleavage

efficiency [15]. For this reason, I used the T2A peptide as a linker for all of the bi-cistronic vectors used in this study.

Although 2A peptides are useful for the simultaneous expression of multiple genes at the same site and have received significant attention in the xenotransplantation field, factors influencing the expression levels of the target genes in a poly-cistronic T2A expression (T2A-Ex) system have not been fully elucidated. Several studies have shown that 2A peptide-mediated gene expression might be influenced by protein cleavage and the positioning of the genes within the vector [20-22]. For example, although most proteins are synthesized in ribosomal complexes, some proteins that localize to the plasma membrane are also integrated within the endoplasmic reticulum (ER) but not in the cytosolic fractions. Therefore, differential subcellular localization might influence the expression pattern of target genes coupled to the 2A peptide.

Because the stable and consistent expression of all of the target genes is essential for xenograft survival, I evaluated the impact of the gene positioning and subcellular localization of target genes on their expression patterns using bi-cistronic T2A-Ex constructs driven by a CMV promoter. The combination of four commonly used genes, including the enhanced green fluorescent protein (EGFP), HA-tagged human heme oxygenase 1 ((HA)HO1), human thrombomodulin (hTBM), and hCD46, were used to determine the protein expression patterns using the T2A-Ex system.

Materials and Methods

Cells and cell culture

Porcine fibroblasts were isolated from White Yucatan miniature pig fetuses on day 35 of gestation as previously described [23]. The cells were kindly provided by Dr. Hyunil Kim and OPTIFARM SOLUTION. The cells were maintained in Dulbecco's modified Eagle medium (DMEM; WelGENE, Daegu, Korea) supplemented with 20% (v/v) fetal bovine serum (FBS; Gibco, MD, USA) and 1% (v/v) antibiotic-antimycotic solution (Gibco, MD, USA) at 38°C in a humidified carbon dioxide-controlled (5%) incubator.

Plasmid construction and transfection

The primers used in this study are summarized in Table 1. For the IRES-related constructs, each upstream gene was inserted into the pIRES vector (Clontech, CA, USA) using NheI and XhoI. After the insertion of the upstream gene, each downstream gene was inserted using BamHI and NotI. In the T2A-Ex constructs, each of the upstream genes except for hTBM was inserted into the pBlue-T2A vector (pBluescript II KS(-) vector including a T2A peptide with an N-terminal furin cleavage sequence at the EcoRV site) using KpnI and EcoRI. The hTBM gene was inserted into the pBlue-T2A vector between the BamHI and EcoRI. Each of downstream genes was inserted using HindIII and XhoI. After the insertion of both upstream and downstream genes, the entire coding region was

subcloned into the pcDNA3.1(+) or pCAG1.1 vectors (in which the CMV promoter was exchanged with the CAG promoter in pcDNA3.1(+) vector) using KpnI and XhoI, or BamHI and XhoI, respectively. The stop codons of all upstream genes were deleted in the bi-cistronic T2A-Ex vector. After construction of the bi-cistronic T2A-Ex vectors, EGFP-T2A-(HA)HO1 and hTBM-T2A-(HA)HO1 sequences were used for construction of the tri-cistronic T2A-Ex vectors. Upstream EGFP-T2A-(HA)HO1 and hTBM-T2A-(HA)HO1 sequences without stop codon were amplified by polymerase chain reaction (PCR) and 5'-regions were digested by KpnI or BamHI, respectively. Downstream T2A-hCD46 sequences were amplified and 3'-region was digested by XhoI. After treatment with T4 poly nucleotide kinase (Elpis Biotech, Daejeon, Korea), upstream and downstream sequences were inserted together into pcDNA3.1(+) using KpnI and XhoI or BamHI and XhoI. The bi-cistronic gene combinations used in this study are summarized in Table 2.

To examine the protein expression pattern of these constructs, 2 (Fig. 2 and 6) or 3 μg (Fig. 1, 3, 4, and 5) of each plasmid were transiently introduced into 1x106 porcine fibroblasts. For RNA interference, I used 1 μg of small interfering RNA (siRNA) targeting GFP or luciferase GL2 (siGFP or siLuc, respectively; GenePharma, Shanghai, China). The sequences of the siRNAs were designated as follows: siGFP, 5'-GGCUACGUCCAGGAGCGCACC-3' and 5'-UGCGCUCCUGGACGUAGCCUU-3', and siLuc, 5'-CGUACGCGGAAUACUUCGAdTdT-3' and 5'-UCGAAGUAUUCCGCGUACGdTdT-3'. For transfection, I electroporated the cells using Nucleofector II™ and the Nucleofector™ Kit V (Lonza, Cologne,

Germany) according to the manufacturer's protocols.

Flow cytometry

Detached cells were incubated in phosphate-buffered saline (PBS; Invitrogen, CA, USA) with 2% (w/v) bovine serum albumin (BSA; Invitrogen, CA, USA) and the indicated antibodies. For intracellular staining, FIX & PERM™ and permeabilization buffers (Invitrogen, CA, USA) were used. For the detection of the HA-epitopes, a mouse anti-HA-Tag antibody (1:200; Abcam, MA, USA) and allophycocyanin (APC)-conjugated goat anti-mouse IgG antibody (1:50; Santa Cruz Biotechnology, CA, USA) were used sequentially. For the detection of hTBM and hCD46, APC-conjugated mouse anti-human TBM (1:100; R&D Systems, MN, USA) and CD46 (1:100; Abcam, MA, USA) antibodies were used, respectively. The immunostained cells were analyzed using a FACSCalibur flow cytometer (Becton Dickinson, CA, USA) with FlowJo software (Tree Star, OR, USA). The levels of the proteins expressed by multiple gene constructs were determined more than three times each and applied for quantitative analysis, as shown in Table 3.

Western blotting

The transfected cells were harvested and lysed in RIPA buffer (BIOSESANG, Seongnam, Korea) supplemented with a protease inhibitor cocktail (Complete Mini; Roche, NJ, USA). Five micrograms of each cell lysate were quantified

using a Bradford assay reagent (BIOSESANG, Korea) and loaded per lane. The lysate samples were resolved using SDS-PAGE and transferred to PVDF membranes (Merck Millipore, MA, USA). The membranes were blocked in TBS containing 0.1% (v/v) Tween-20 (TBST; Bio-Rad, CA, USA) and 5% (w/v) skim milk (Becton Dickinson, CA, USA). After 1 hour of blocking at room temperature, the membranes were sequentially incubated with the indicated primary and secondary antibodies diluted in TBST containing 2% (w/v) BSA (Invitrogen, CA, USA). The following primary antibodies were used for immunoblotting: mouse anti-GFP antibody (1:5000; Santa Cruz Biotechnology, CA, USA), mouse anti-HA-Tag antibody (1:4000; Abcam, MA, USA), mouse anti-Myc-Tag antibody (1:2000; Cell Signaling, MA, USA), mouse anti-hTBM antibody (1:1000; Abcam, MA, USA), and rabbit anti-hCD46 antibody (1:1000; Abcam, MA, USA). The following secondary antibodies were used for immunoblotting: horseradish peroxidase (HRP)-conjugated goat anti-mouse IgG (1:10000; AbFrontier, Seoul, Korea) and HRP-conjugated goat anti-rabbit IgG (1:5000; AbFrontier, Seoul, Korea). After three washes with TBST, chemiluminescent detection was performed using the AbSignal™ Kit (AbClon, Seoul, Korea), followed by X-ray film exposure.

Fluorescent microscopy

Coverslips were incubated with 0.01% (w/v) poly-L-lysine solution (Sigma, MO, USA) for 1 hour. After washing with 70% ethanol, the coverslips were placed into the individual wells of a six-well plate. Ten thousand transfected cells were

seeded into each well. After washing twice with 1X PBS, the cells were fixed with 3.7% (w/v) paraformaldehyde at room temperature for 30 minutes. After washing with 1X PBS, the cells were incubated with 2 μg/ml of Hoechst 33342 at room temperature for 10 minutes to stain the nuclei (DNA) of the cells. After three washes with 1X PBS, GFP expression and Hoechst 33342 were examined using a Zeiss LSM 410 confocal microscope (Carl Zeiss AG, Oberkochen, Germany).

RNA isolation and semi-quantitative reverse transcription polymerase chain reaction

Total RNA was isolated from the transfected cells using the RNeasy™ Mini Kit (Qiagen, CA, USA) according to the manufacturer's protocols. To remove the residual plasmid DNA, 1 mg of total RNA was incubated with 0.2 units of RQ1 RNase-Free DNase (Promega, WI, USA) at 37°C for 30 minutes. After the addition of 0.2 μl of RQ1 DNase Stop Solution, the samples were incubated at 65°C for 10 minutes to inactivate the DNase. After the removal of the residual plasmid DNA, the total RNA was reverse transcribed into complementary DNA (cDNA) using SuperScript™ III Reverse Transcriptase (Invitrogen, CA, USA) according to the manufacturer's protocols. Next, 23 cycles of polymerase chain reaction (PCR) were performed using a PCR Thermal Cycler Dice™ (TAKARA, Shiga, Japan) and HiPi Thermostable DNA Polymerase (Elpis Biotech, Daejeon, Korea) with the EGFP or β-Actin primer pairs summarized in Table 1. The PCR products were electrophoresed on 1.5% (w/v) agarose gels in 0.5X TBE buffer

and visualized by UV transillumination.

Statistical analysis

The SPSS version 18.0 (SPSS Inc., IL, USA) was used for statistical analysis. Unpaired Student's t-test was used to compare results between groups. P-values less than 0.05 were considered statistically significant (*, $p<0.05$; **, $p<0.01$; ***, $p<0.001$; ns, not significant). Error bars represent standard error of the mean.

Results

IRES-dependent downstream genes are not efficiently expressed

It has been well established that the IRES sequence does not produce efficient gene expression in mammalian cells [8, 9]. To resolve this issue, I used the bi-cistronic IRES expression (IRES-Ex) system shown in Figure 1A. I constructed two bi-cistronic IRES-Ex vectors containing upstream and downstream combinations of the EGFP and (HA)HO1 genes and introduced each construct into porcine fibroblasts. Using flow cytometric analysis, I found that the expression levels of the downstream EGFP and (HA)HO1 genes were significantly reduced compared with those of the upstream EGFP and (HA)HO1 genes (Fig. 1B). The expression levels of both genes were also confirmed by immunoblot analysis using the antibodies specific for each gene. Consistent with the flow cytometric results, the expression of the downstream EGFP and (HA)HO1 was barely detectable (Fig. 1C).

The position of the target gene within the T2A-Ex vector does not affect its expression levels

A schematic diagram of the bi-cistronic T2A-Ex constructs is presented in Figure 2A. To compare the expression levels of the upstream genes with those of downstream genes, either HA- or Myc-tagged EGFP ((HA)EGFP or (Myc)EGFP) were used. First, I constructed two mono-cistronic vectors containing either the

(HA)EGFP or (Myc)EGFP sequences and confirmed similar levels of EGFP expression by flow cytometry. Next, bi-cistronic vectors containing (HA)EGFP-T2A-(Myc)EGFP or (Myc)EGFP-T2A-(HA)EGFP sequences were generated. Flow cytometric analysis using porcine fibroblasts transfected with each bi-cistronic vector revealed that both constructs produced similar EGFP signals. However, these signals were stronger than those of the mono-cistronic vectors, suggesting that two copies of the EGFP gene in a single transcript resulted in increased protein synthesis compared to one copy (Fig. 2B). The expression levels of both upstream and downstream EGFP genes were further confirmed by immunoblot analysis. The data showed that the expression levels of the downstream EGFP were similar to those of the upstream EGFP and the EGFP derived from mono-cistronic vector. Tagging using different epitopes did not affect EGFP expression levels (Fig. 2C).

The combination of genes targeted for different subcellular regions does not influence the protein expression efficiency in the T2A-Ex system

To explore whether the targeting of genes to different subcellular locations can influence the expression patterns of multigene, I generated six bi-cistronic T2A-Ex vectors containing combinations of two intracellular proteins, EGFP and (HA)HO1, and two trans-membrane proteins, hTBM and hCD46.

Immunostaining with an anti-HA antibody, followed by flow cytometric analysis, showed that (HA)HO1 was expressed relatively efficiently, regardless of its position within the bi-cistronic T2A-Ex construct. The EGFP signals were

rather different according its sequence position. When the EGFP gene was located within the downstream region, its expression levels were quite reduced compared with those of the EGFP gene within the upstream region (Fig. 3A). However, compared with the bi-cistronic IRES-Ex construct (Fig. 1B and 1C), the bi-cistronic T2A-Ex construct maintained significantly high expression of each gene within the downstream position (EGFP, $p=0.022$; (HA)HO1, $p=0.009$; data not shown). These results were confirmed by immunoblot analysis. Both the EGFP and (HA)HO1 proteins were clearly detectable, regardless of their position within the bi-cistronic T2A-Ex construct, even though the signal of the downstream EGFP was negligibly weaker than that of the upstream EGFP. The molecular sizes of the upstream genes were slightly larger due to the addition of a C-terminal T2A peptide, indicating that furin-dependent cleavage did not occur in the cytosol, although the protease target site was inserted upstream of T2A peptide (Fig. 3B).

The expression pattern of the two trans-membrane molecules, hTBM and hCD46, were examined using the bi-cistronic T2A-Ex constructs containing the hTBM-T2A-hCD46 or hCD46-T2A-hTBM sequences, respectively. The porcine fibroblasts transfected with the hTBM-T2A-hCD46 vector expressed both hTBM and hCD46 proteins at the cell surface. However, in flow cytometric analysis with the hCD46-T2A-hTBM-transfected cells, the protein expression levels of both hCD46 and hTBM were extremely low compared with hTBM-T2A-hCD46-transfected cells. Similar to this, they were undetectable in western blotting (Fig. 3C and 3D).

To evaluate the expression of the combined genes in the context of different

subcellular localization, bi-cistronic T2A-Ex constructs containing either EGFP-T2A-hTBM or hTBM-T2A-EGFP sequences were generated. Flow cytometric analysis showed that both EGFP and hTBM proteins were well expressed at their differential subcellular locations. Interestingly, however, the protein expression levels of both genes were quite different between the groups (Fig. 3E). Immunoblot analysis showed that the upstream EGFP was present at an increased size due to the addition of the T2A peptide. However, the upstream hTBM was detected at its original size due to cleavage by furin, which is present in the ER lumen (Fig. 3F).

The influence of upstream gene expression on downstream gene expression in the T2A-Ex constructs

In Figure 3A, reduced EGFP expression was observed when the EGFP gene was located within the downstream region. The expression of the EGFP protein was also decreased when the EGFP gene was located within the downstream region of the hTBM gene (Fig. 3E). Moreover, in hCD46-T2A-hTBM-transfected cells, negligible expression of hTBM protein was observed, although when the hTBM gene was located in the upstream position or in the mono-cistronic vector, it was highly expressed (Fig. 3C and data not shown). Interestingly, hCD46 was expressed efficiently by the T2A-Ex construct containing hTBM-T2A-hCD46, whereas when the hCD46 gene was located in the upstream position or in the mono-cistronic vector, it was not efficiently expressed. In this study, I used a CMV promoter-derived gene expression system. The other genes were expressed

efficiently by this promoter. However, the hCD46 gene was not expressed efficiently. To determine the promoter dependency of the hCD46 gene, I subcloned hCD46-T2A-hTBM sequences into a chicken β-actin (CAG) promoter-containing vector. Because the upstream hCD46 gene was expressed efficiently under the control of the CAG promoter, the downstream hTBM gene was also expressed efficiently. The protein expression levels of both genes were not different from hTBM-T2A-hCD46-transfected group in CAG promoter-driven expression system (Fig. 3C and 3D). These findings suggest that the expression efficiency of the upstream genes may influence the expression efficiency of the downstream genes.

To exclude the interference of different antibody binding affinities, I generated a structural sequence of Gene A–T2A–EGFP. After inserting the three different genes ((HA)HO1, hTBM, and hCD46) into the Gene A position, each bi-cistronic vector was introduced into porcine fibroblasts, and the mean fluorescent intensity (MFI) of EGFP was measured by flow cytometry. The EGFP expression levels decreased in order of combination with (HA)HO1, hTBM, and hCD46 (Fig. 4A). The EGFP signals from each construct observed by fluorescence microscopy were correlated with the flow cytometry results (Fig. 4B). To identify whether different protein expression levels of the downstream EGFP gene were correlated with the mRNA expression levels, I assessed the mRNA levels using reverse transcription polymerase chain reaction (RT-PCR) for EGFP because all of the constructs contained EGFP sequences at the same position. The data showed that different amounts of the mRNA existed in each group and that the mRNA levels were significantly correlated with the protein levels (Fig. 4C). The different

mRNA levels might be due to the transcriptional efficiency of each construct or the stability of the transcripts.

To determine whether the expression levels of the downstream genes were influenced by those of upstream genes in the context of subcellular localization, EGFP and hTMB were selected as upstream genes because EGFP expressed much more efficiently than hTBM in this system. (HA)HO1 and hCD46 were used as the downstream genes. The expression levels of EGFP and hTBM were consistent and not influenced by the downstream genes. However, (HA)HO1 and hCD46 were expressed much more efficiently when EGFP was positioned within the upstream region compared with hTMB (Fig. 5A and 5B). To investigate if expression efficiency of the first gene influences downstream gene expression in triple gene construct, I developed tri-cistronic T2A-Ex system with combination of EGFP-T2A-(HA)HO1-T2A-hCD46 or hTBM-T2A-(HA)HO1-T2A-hCD46. Flow cytometric analysis and western blotting data showed that expression levels of hCD46 in the third position were also related to the expression efficiency of the first gene (EGFP or hTBM). Furthermore, the expression levels of hCD46 in the third position were quite similar to those of hCD46 in second position of bi-cistronic construct (Fig. 5A and 5B).

These results indicate that the expression level of downstream genes appears to be dependent on the transcriptional efficiency of upstream genes in the T2A-Ex constructs, regardless of their targeted subcellular localization.

Multigene expression driven by a single promoter can be regulated by RNA interference of one gene member

Small RNAs can bind to specific regions of gene transcripts with which they share significant homology, resulting in the degradation or translational disruption of the transcripts, a phenomenon called RNA interference [24, 25]. Because the poly-cistronic T2A-Ex construct produces a single transcript containing multiple genes, a microRNA (miRNA) targeting one gene within the transcript would simultaneously downregulate the expression of the other genes.

To examine the effects of RNA interference on the bi-cistronic T2A-Ex constructs, I introduced each bi-cistronic vector (EGFP–T2A–hTBM or hTBM–T2A–EGFP) into porcine fibroblasts simultaneously with EGFP-targeted siRNA (siGFP). Flow cytometric analysis showed that the EGFP signals from both constructs were significantly decreased by siGFP, indicating that the siRNA efficiently downregulated the expression of the target gene. The expression levels of either the upstream- or downstream-positioned hTBM gene were also decreased (Fig. 6A). Western blotting with specific antibodies confirmed that the expression of both proteins was markedly decreased (Fig. 6B). In addition, I assessed the mRNA levels of EGPF using RT-PCR and found that both transcripts were significantly reduced by siGFP (Fig. 6C). These results demonstrate that an siRNA targeting a single gene within the multigene transcript can also affect the expression of the other genes.

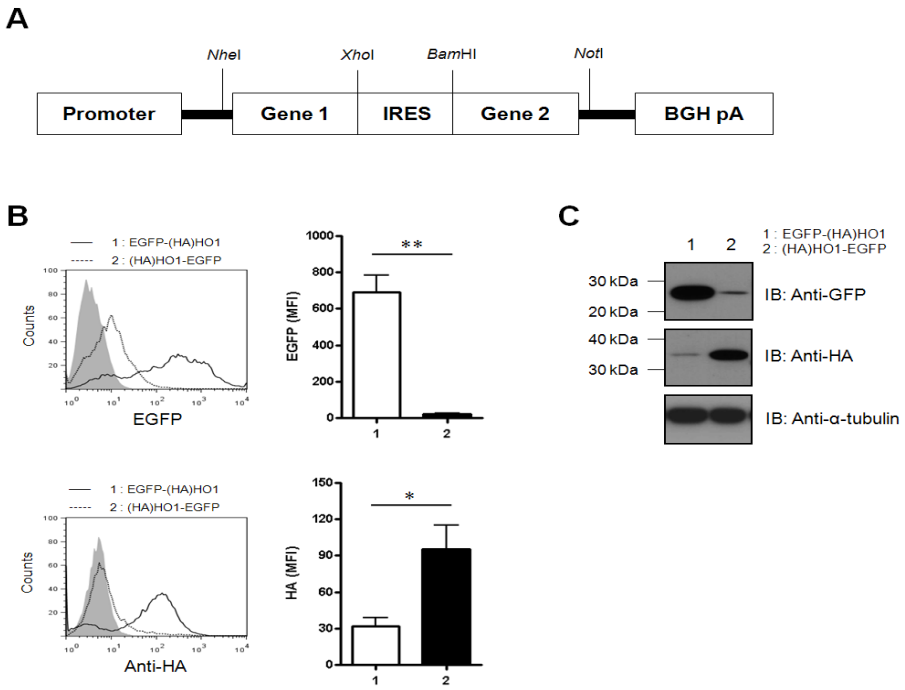

Figure 1. The expression levels of downstream genes are extremely low in the bi-cistronic IRES-Ex constructs.

A) Schematic diagram of the bi-cistronic IRES-Ex vector. B) Porcine fibroblasts were transfected with the vector containing the EGFP-IRES-(HA)HO1 or (HA)HO1-IRES-EGFP sequences. The cells were analyzed using flow cytometry at 24 h after transfection. For (HA)HO1 detection, the cells were incubated with the mouse anti-HA Ab, followed by the APC-conjugated goat anti-mouse IgG Ab, according to the intracellular staining protocol. Mock transfected cells were used as control (filled line). Summarized bar graphs show means ± SE of three independent replications. C) The cell lysates were subjected to immunoblotting with either the mouse anti-GFP or mouse anti-HA Abs, followed by HRP-conjugated goat anti-mouse IgG. These results are representative of three independent experiments.

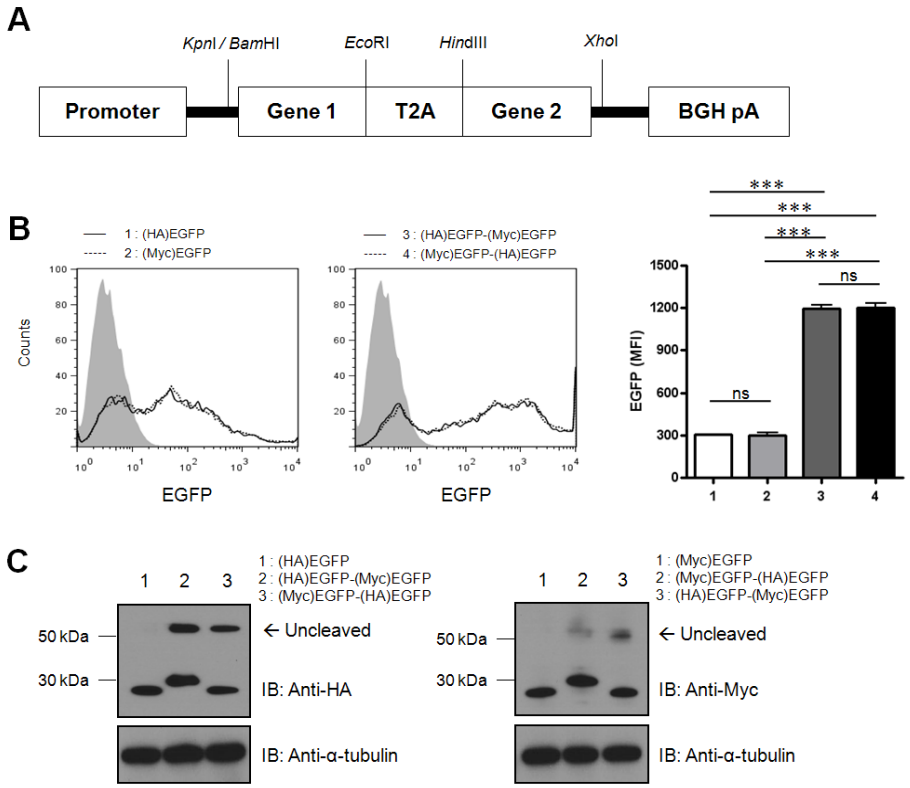

Figure 2. The expression levels of downstream genes are approximately equivalent to those of upstream genes.

A) Schematic diagram of bi-cistronic T2A-Ex. B) Porcine fibroblasts were transfected with vector containing a single gene, (HA)EGFP or (Myc)EGFP, or vector containing a combination of genes, (HA)EGFP-T2A-(Myc)EGFP or (Myc)EGFP-T2A-(HA)EGFP. At 24 h after transfection, the EGFP signals were analyzed by flow cytometry. Mock transfected cells were used as control (filled line). Summarized bar graphs show means ± SE of three independent replications. C) The cell lysates were examined by immunoblot analysis with the mouse anti-HA or mouse anti-Myc Abs, followed by the HRP-conjugated goat anti-mouse IgG. These results are representative of three independent experiments.

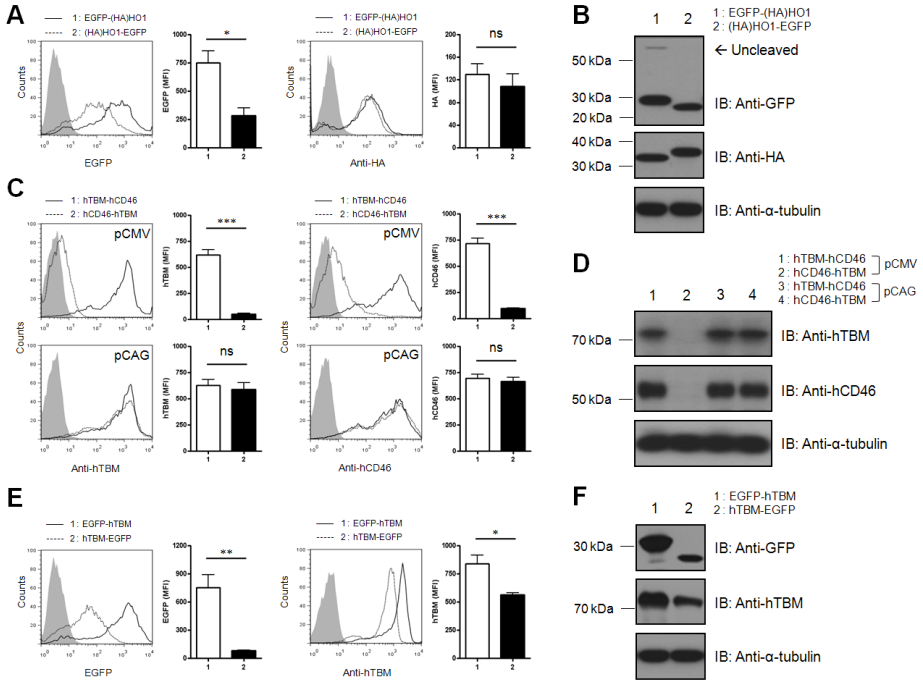

Figure 3. Both genes in the bi-cistronic T2A-Ex constructs are localized efficiently to their subcellular location.

A-B) The bi-cistronic T2A-Ex vector containing the EGFP-T2A-(HA)HO1 or (HA)HO1-T2A-EGFP sequences was introduced into porcine fibroblasts, and the expression patterns of each gene were analyzed by flow cytometry (A) and western blotting (B) with the indicated antibodies. Mock transfected cells were used as control (filled line). Summarized bar graphs show means ± SE of four independent replications. C) Porcine fibroblasts transfected with CMV- (upper panel) or CAG-based (lower panel) bi-cistronic T2A-Ex vector containing the hTBM-T2A-hCD46 or hCD46-T2A-hTBM sequences. The cell surface expression of hTBM or hCD46 was analyzed by flow cytometry using the APC-conjugated mouse anti-hTBM or APC-conjugated mouse anti-hCD46 antibodies, respectively. Mock transfected cells were used as control (filled line).

Summarized bar graphs show means ± SE of three independent replications. D) The cell lysates were subjected to immunoblotting with the mouse anti-hTBM and rabbit anti-hCD46 antibodies, followed by the HRP-conjugated goat anti-mouse IgG or HRP-conjugated goat anti-rabbit IgG, respectively. E-F) The expression patterns of target genes in the porcine fibroblasts transfected with the bi-cistronic T2A-Ex vector containing the EGFP-T2A-hTBM or hTBM-T2A-EGFP sequences were analyzed by flow cytometry (E) and western blotting (F) with the indicated antibodies. Mock transfected cells were used as control (filled line). Summarized bar graphs show means ± SE of four independent replications. These results are representative of more than three independent experiments.

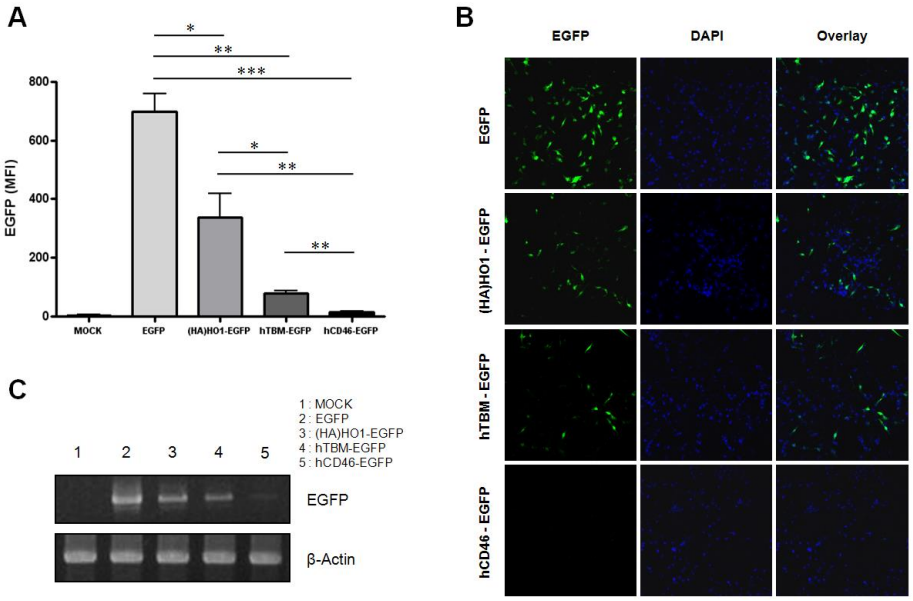

Figure 4. The downstream gene expression levels are correlated with the transcriptional efficiency of the upstream gene.

A) Porcine fibroblasts were transfected with each indicated vector, and the mean fluorescent intensity (MFI) of EGFP was analyzed by flow cytometry. Summarized bar graphs show means ± SE of three independent replications. B) The expression levels and the subcellular localization of EGFP were analyzed using a fluorescent microscope. Hoechst 33342 was used for nuclear staining (original magnification X200). C) After the removal of the residual plasmid DNA with DNase treatment, the RNA extracts were subjected to RT-PCR for EGFP. These results are representative of three independent experiments.

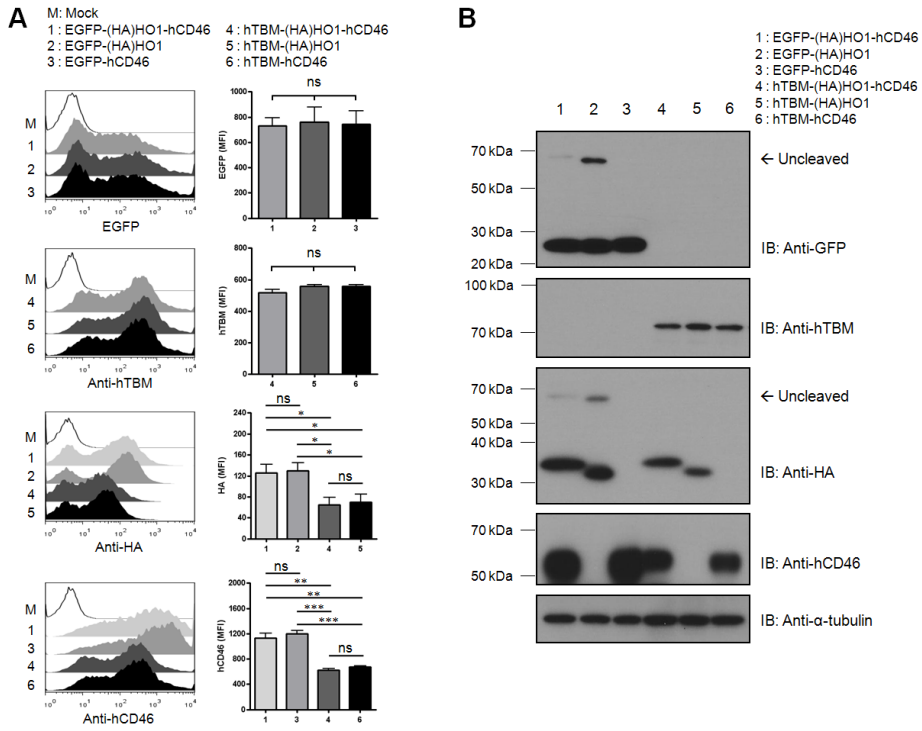

Figure 5. The expression levels of each gene are not related with differences in subcellular localization.

A-B) The bi- and tri-cistronic T2A-Ex vectors containing the indicated gene combinations were introduced into porcine fibroblasts. The expression levels of each gene were analyzed by flow cytometry (A) and western blotting (B) with the indicated antibodies. Summarized bar graphs show means ± SE of four independent replications. These results are representative of four independent experiments.

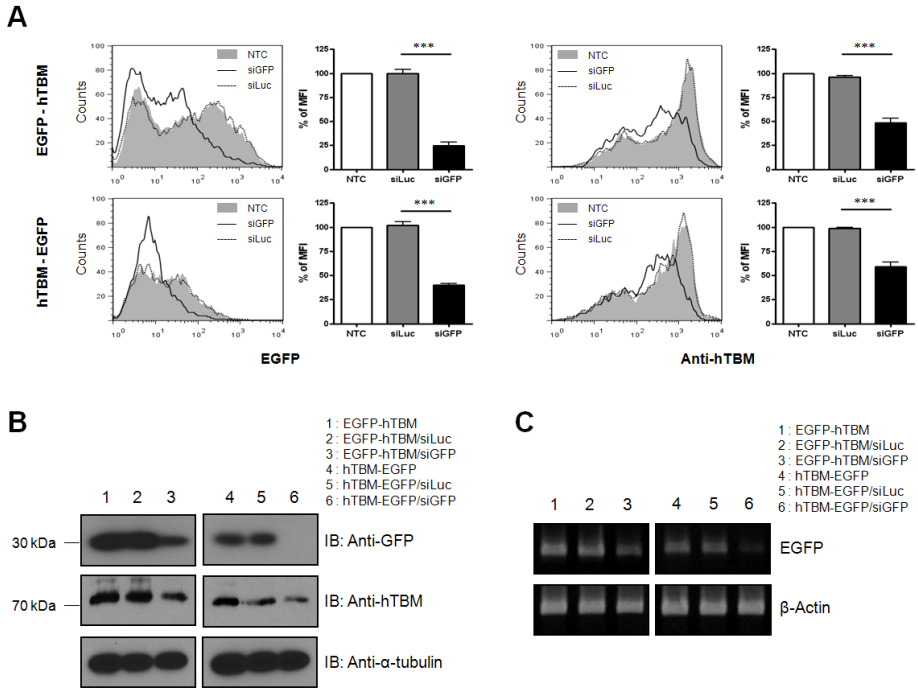

Figure 6. The siRNA targeting of one gene can downregulate both genes in bi-cistronic T2A-Ex constructs.

A) Porcine fibroblasts were cotransfected with the bi-cistronic vector containing EGFP-T2A-hTBM or hTBM-T2A-EGFP and siRNA targeting EGFP sequence. The expression levels of each gene were analyzed by flow cytometry at 24 h after cotransfection. Summarized bar graphs show means ± SE of three independent replications. B) The cell lysates were subjected to western blotting. C) After DNase treatment for the removal of residual plasmid DNA, the RNA extracts were subjected to RT-PCR analysis for EGFP. NTC, non-treated cells; siLuc, control siRNA-treated cells; siGFP, target siRNA-treated cells. These results are representative of three independent experiments.

Table 1. The primer sets used for plasmid construction and RT-PCR.

Purpose	Primer name	Primer sequence (5'-3')
Plasmid Construction	EGFP forward (*Nhe* I)	AAGCTAGCACCATGGTGAGCAAGGGCGAGG
	EGFP reverse (*Xho* I)	ATCTCGAGTTACTTGTACAGCTCGTCC
	EGFP forward (*Bam*H I)	AAGGATCCATGGTGAGCAAGGGCGAGG
	EGFP reverse (*Not* I)	AAATTGCGGCCGCTTACTTGTACAGCTCGTCC
	(HA)HO1 forward (*Nhe* I)	AAGCTAGCACCATGTACCCATACGATGTTCCAGA TTACGCTATGGAGCGTCCGCAACCCG
	hHO1 reverse (*Xho* I)	ATCTCGAGTCACATGGCATAAAGCCC
	HA forward (*Bam*H I)	AAGGATCCATGTACCCATACGATGTTC
	hHO1 reverse (*Not* I)	AAATTGCGGCCGCTCACATGGCATAAAGCCC
	EGFP forward (*Kpn* I)	AAGGTACCATGGTGAGCAAGGGCGAGG
	HA reverse (Δstop, *Eco*R I)	TTGAATTCAGCGTAATCTGGAACATCG
	EGFP forward (*Hin*d III)	ATAAGCTTATGGTGAGCAAGGGCGAGG
	(HA)EGFP reverse (*Xho* I)	AACTCGAGTTAAGCGTAATCTGGAACATCGTATG GGTACTTGTACAGCTCGTCCATGC
	Myc reverse (Δstop, *Eco*R I)	TTGAATTCCAGGTCCTCCTCTGAGATC
	(Myc)EGFP reverse (*Xho* I)	AACTCGAGTTACAGGTCCTCCTCTGAGATCAGCT TCTGCTCCTTGTACAGCTCGTCCATGC
	HA forward (*Kpn* I)	AAGGTACCATGTACCCATACGATGTTC

	hHO1 reverse (Δstop, *Eco*R I)	**AAGAATTCCATGGCATAAAGCCCTAC**
	HA forward (*Hin*d III)	**ATAAGCTTATGTACCCATACGATGTTC**
	hTBM forward (*Bam*H I)	**AAGGATCCACCATGCTTGGGGTCCTGGTCC**
	hTBM reverse (Δstop, *Eco*R I)	**ATGAATTCGAGTCTCTGCGGCGTCCGC**
	hTBM forward (*Hin*d III)	**ATAAGCTTATGCTTGGGGTCCTGGTCC**
	hTBM reverse (*Xho* I)	**ATCTCGAGTCAGAGTCTCTGCGGCGTC**
	hCD46 forward (*Kpn* I)	**AAGGTACCATGGAGCCTCCCGGCCGCC**
	hCD46 reverse (Δstop, *Eco*R I)	**AAGAATTCGAGAGAAGTAAATTTTAC**
	hCD46 forward (*Hin*d III)	**ATAAGCTTATGGAGCCTCCCGGCCGCC**
	hCD46 reverse (*Xho* I)	**ATCTCGAGTCAGAGAGAAGTAAATTTTAC**
RT-PCR	**EGFP forward**	**ATGGTGAGCAAGGGCGAGG**
	EGFP reverse	**TTACTTGTACAGCTCGTCC**
	β-actin forward	**ATCTGGCACCACACCTTCTACAATGAGCTGCG**
	β-actin reverse	**CGTCATACTCCTGCTTGCTGATCCACATCTGC**

Table 2. The combinations of target genes within the bi-cistronic T2A-Ex vector.

Promoter	Gene A	-	Gene B	Verification
CMV[1]	(HA)EGFP[2]	-	(Myc)EGFP	Position
	(Myc)EGFP	-	(HA)EGFP	
	EGFP	-	(HA)HO1[3]	Intracellular Protein
	(HA)HO1	-	EGFP	
	hTBM[4]	-	hCD46[5]	Transmembrane Protein
	hCD46	-	hTBM	
	EGFP	-	hTBM	Mixed
	hTBM	-	EGFP	
	hCD46	-	EGFP	
	EGFP	-	hCD46	
	hTBM	-	(HA)HO1	

[1]Cytomegalovirus

[2]Enhanced green fluorescent protein

[3]Human heme oxygenase 1

[4]Human thrombomodulin

[5]Human cluster of differentiation 46

Table 3. The quantitative analysis of each gene by multi-cistronic vectors used in this study.

Promoter	Gene Combination	Linker	N	MFI (Mean ± SE)			
				EGFP	(HA)HO1	hTBM	hCD46
CMV	EGFP–(HA)HO1	IRES	3	690.0 ± 95.7	31.9 ± 6.7		
	(HA)HO1–EGFP	IRES	3	21.1 ± 3.9	95.5 ± 19.7		
	EGFP–(HA)HO1	T2A	8	755.6 ± 74.0	129.6 ± 11.4		
	(HA)HO1–EGFP	T2A	7	306.3 ± 48.8	109.0 ± 13.3		
	hTBM–hCD46	T2A	7			584.5 ± 23.8	690.0 ± 24.8
	hCD46–hTBM	T2A	3			53.6 ± 5.2	96.5 ± 7.6

	EGFP–hTBM	**T2A**	**4**	**752.6 ± 135.0**		**840.2 ± 73.0**	
	hTBM–EGFP	**T2A**	**7**	**79.2 ± 4.3**		**563.9 ± 11.2**	
	hCD46–EGFP	**T2A**	**3**	**13.1 ± 2.9**			**85.4 ± 12.8**
	EGFP–hCD46	**T2A**	**4**	**742.1 ± 108.9**			**1201.4 ± 50.4**
	hTBM–(HA)HO1	**T2A**	**4**		**69.8 ± 15.7**	**558.9 ± 9.8**	
	EGFP–(HA)HO1–hCD46	**T2A**	**4**	**729.7 ± 63.9**	**125.8 ± 16.1**		**1128.1 ± 84.2**
	hTBM–(HA)HO1–hCD46	**T2A**	**4**		**64.3 ± 14.7**	**516.5 ± 21.2**	**627.1 ± 25.7**

Discussion

The crossing of different transgenic pigs has long been considered the simplest approach to generate multiple transgenic pigs. Recently, however, a viral gene expression system using a 2A peptide sequence has highlighted a novel, practical method to establish multiple transgenic animals. In the context of poly-cistronic expression systems, 2A peptides have been successfully applied in several research fields, including the generation of induced pluripotent stem (iPS) cells from somatic cells [26-28], the generation of therapeutic antibody-producing cells [29], and the correction of multigene deficiencies [17]. In addition, generations of multiple transgenic animals using 2A peptides have been previously reported [30-33]. However, nobody tried to investigate expression efficiency of the each gene in multi-gene expression system depending on the position.

In terms of generating multiple transgenic pigs, double-transgenic pigs produced by the crossing of hDAF x hCD59 transgenic lines produced heterogeneous gene expression [34]. In triple-transgenic pigs produced by the serial integration of each gene, the expression levels of the transgenes were significantly variable between different tissues, and furthermore, some were not detectably expressed in certain tissues [4]. These observations might be attributed to the different integration loci of each transgene or differences in the promoter control of the genes. The 2A peptide-dependent gene expression system represents a viable alternative to solve this problem. 2A peptide-based multiple transgenic pigs have previously exhibited optimal co-expression of four fluorescent proteins in various tissues [33], indicating that poly-cistronic T2A-Ex system represents an attractive tool for the generation of multiple transgenic pigs,

even though the tissue-dependent regulation of promoter activity still must be resolved to ensure that the transgenes are homogenously expressed.

Several reports have suggested that the expression of multiple genes coupled with a 2A peptide is more efficient than IRES-based expression system [31, 35]. Fisicaro et al. reported that a 2A peptide-based tetra-cistronic plasmid did not exhibit any decreased expression of the target genes compared with bi- or tri-cistronic plasmids, at least in vitro [36]. In the experiments using EGFP with different epitope-tagging (HA or Myc), I also identified that the expression levels of the downstream gene were similar to that of upstream gene in the T2A-Ex constructs. However, to be a prospective tool for establishing multiple transgenic animals, the expression patterns of target genes exhibiting different behaviors, including subcellular localization, together with the positional effect of the genes and promoter usage, should be evaluated using the T2A-Ex vector.

This study using several T2A-Ex constructs revealed that the downstream gene expression likely depends on the expression efficiency of the upstream gene. As demonstrated in this experiment using the Gene A–T2A–EGFP constructs, the protein amount of each downstream EGFP gene was measured by MFI, and it correlated with the expression level of the upstream genes. Because the MFI of the downstream EGFP was significantly correlated with its mRNA expression level, which reflected the relative expression level of the upstream gene, the expression levels of downstream gene appeared to be dependent on the transcriptional efficiency of upstream gene. I next confirmed the influence of the expression efficiency of the upstream gene on the expression efficiency of the downstream gene. The downstream-positioned (HA)HO1 and hCD46 genes were

expressed in an upstream gene-dependent manner. Because EGFP was highly expressed compared with hTBM, downstream (HA)HO1 and hCD46 combined with upstream EGFP were also highly expressed compared with the hTBM combination. When the hCD46 gene was positioned upstream of the T2A-Ex construct, the protein expression was barely detected, similar to the expression exhibited by the mono-cistronic vector containing hCD46 alone. Interestingly, the expression of the downstream EGFP and hTBM combined with hCD46 was dramatically decreased. Next, I exchanged the CMV promoter with the CAG promoter to evaluate the extent of promoter dependency on hCD46 expression. The CAG promoter was sufficient to induce hCD46 expression, and the expression of the upstream hCD46 was accompanied by the expression of the downstream hTBM.

Because proteins targeted for different subcellular compartments can be synthesized by different machinery, the differential subcellular targeting might influence the expression of the multiple genes expressed from the same T2A-Ex construct. However, the experiment with the combination of cytosolic EGFP and plasma membrane-targeted hTBM indicated that the two genes were efficiently expressed, regardless of targeted localization. Rather, their expression was affected by the transcriptional efficiency of the upstream gene. Moreover, especially in flow cytometric analysis, the range of difference for EGFP was more extensive than that for hTBM between the groups and it suggests that the degree of antibody binding affinity may attenuate the range of difference between the groups. Accordingly, the fluorescence intensity of EGFP appears to be able to distinguish the change of protein expression levels exquisitely. For this reason,

EGFP was used as a downstream gene for comparing the expression efficiency of upstream genes effectively regardless of interference of different antibody binding affinities. Alternatively, immunoblot analyses performed in parallel with flow cytometric analysis precisely reflect the expression change of EGFP and hTBM depending on the position of the genes in T2A-Ex system.

Recently, Kim et al. evaluated the cleavage efficiency of four different 2A peptides and showed that the subcellular localization of the protein was influenced by cleavage efficiency [16]. In this study, I detected small amounts of uncleaved peptide when the EGFP gene was positioned within the upstream region. Nevertheless, the uncleaved form was not detected when the gene encoding the transmembrane protein was located within downstream region (Fig. 2C, 3B, 3F, and 5B). These data suggested that the minimal uncleaved form might be cleared by the furin cleavage system within the ER [37] or by signal peptide cleavage of the type I transmembrane protein [38]. Consistent with this notion, flow cytometric analysis showed that the transmembrane proteins were efficiently expressed on the cell surface in all cases. In addition, fluorescent microscopy also showed that EGFP positioned either upstream or downstream of the T2A peptide was expressed efficiently in the cytosol, regardless of the targeted localization of the other genes. Consistent with this results, previous studies have shown that an uncleaved form was readily observed using the same EGFP-containing constructs [15, 39, 40]. This result might be attributed to the expression of a large number of mRNA when the EGFP gene is positioned within the upstream region. To clarify this issue, however, diverse gene combinations must be evaluated in various cell types.

RNA interference represents a useful mechanism that produces various cellular phenotypes with limited gene numbers by targeting specific genes to inhibit their expression in cellular- or tissue-specific contexts. Using in situ miRNA regulation, Brown et al. [41] induced the systemic transduction of lentiviral vectors encoding for transgenes with target sequences of endogenous miRNAs and demonstrated the possibility of using miRNAs in segregating transgene expression between different tissues. Endogenous miRNAs commonly recognize the seed region of 3'-untranslated regions (3'-UTRs) of mRNAs [42]. In a recent study, however, Tay et al. [43] demonstrated that endogenous miRNAs can also react with the coding regions of target genes. To examine the effects of endogenously occurring miRNAs on the T2A-Ex constructs, I used siRNAs that targeted the coding sequence of one transgene. The siRNA significantly downregulated the expression of both the specific target gene and the other gene in the T2A-Ex construct, regardless of their position within the vector. Because both genes are transcribed as one mRNA transcript driven by a single promoter, the overall expression of the genes contained within the T2A-Ex construct was expected to be regulated by the single gene-targeted siRNA. Therefore, RNA interference should be considered another factor for transgene selection in a poly-cistronic expression system, such as T2A-Ex system.

In this study, I tested several combinations of genes in the bi-cistronic T2A-Ex vector in porcine fibroblasts and demonstrated that T2A-Ex is a useful system for efficiently expressing multiple target genes, which likely depends on the adequate expression level of the upstream gene. I also found that the target genes were expressed efficiently, even if they were targeted to different subcellular regions.

Therefore, the T2A-Ex system is a promising tool for generating transgenic pigs that express multiple target genes for xenotransplantation.

References

1. Yang YG, Sykes M. Xenotransplantation: current status and a perspective on the future. Nature reviews. Immunology. 2007;7(7):519-531.

2. Lin CC, Ezzelarab M, Shapiro R, et al. Recipient tissue factor expression is associated with consumptive coagulopathy in pig-to-primate kidney xenotransplantation. American journal of transplantation : official journal of the American Society of Transplantation and the American Society of Transplant Surgeons. 2010;10(7):1556-1568.

3. Le Bas-Bernardet S, Tillou X, Poirier N, et al. Xenotransplantation of galactosyl-transferase knockout, CD55, CD59, CD39, and fucosyl-transferase transgenic pig kidneys into baboons. Transplantation proceedings. 2011;43(9):3426-3430.

4. Zhou CY, McInnes E, Copeman L, et al. Transgenic pigs expressing human CD59, in combination with human membrane cofactor protein and human decay-accelerating factor. Xenotransplantation. 2005;12(2):142-148.

5. Cowan PJ, Aminian A, Barlow H, et al. Renal xenografts from triple-transgenic pigs are not hyperacutely rejected but cause coagulopathy in non-immunosuppressed baboons. Transplantation. 2000;69(12):2504-2515.

6. Webster NL, Forni M, Bacci ML, et al. Multi-transgenic pigs expressing three fluorescent proteins produced with high efficiency by sperm mediated gene transfer. Molecular reproduction and development. 2005;72(1):68-76.

7. Hellen CU, Sarnow P. Internal ribosome entry sites in eukaryotic mRNA

molecules. Genes & development. 2001;15(13):1593-1612.

8. Mizuguchi H, Xu Z, Ishii-Watabe A, Uchida E, Hayakawa T. IRES-dependent second gene expression is significantly lower than cap-dependent first gene expression in a bicistronic vector. Molecular therapy : the journal of the American Society of Gene Therapy. 2000;1(4):376-382.

9. Zhou Y, Aran J, Gottesman MM, Pastan I. Co-expression of human adenosine deaminase and multidrug resistance using a bicistronic retroviral vector. Human gene therapy. 1998;9(3):287-293.

10. Borman AM, Le Mercier P, Girard M, Kean KM. Comparison of picornaviral IRES-driven internal initiation of translation in cultured cells of different origins. Nucleic acids research. 1997;25(5):925-932.

11. Roberts LO, Seamons RA, Belsham GJ. Recognition of picornavirus internal ribosome entry sites within cells; influence of cellular and viral proteins. RNA (New York, N.Y.). 1998;4(5):520-529.

12. de Felipe P. Polycistronic viral vectors. Current gene therapy. 2002;2(3):355-378.

13. Licursi M, Christian SL, Pongnopparat T, Hirasawa K. In vitro and in vivo comparison of viral and cellular internal ribosome entry sites for bicistronic vector expression. Gene therapy. 2011;18(6):631-636.

14. Doronina VA, Wu C, de Felipe P, Sachs MS, Ryan MD, Brown JD. Site-specific release of nascent chains from ribosomes at a sense codon. Molecular and cellular biology. 2008;28(13):4227-4239.

15. Donnelly ML, Hughes LE, Luke G, et al. The 'cleavage' activities of foot-and-mouth disease virus 2A site-directed mutants and naturally occurring '2A-like' sequences. The Journal of general virology. 2001;82(Pt 5):1027-1041.

16. Kim JH, Lee SR, Li LH, et al. High cleavage efficiency of a 2A peptide derived from porcine teschovirus-1 in human cell lines, zebrafish and mice. PloS one. 2011;6(4):e18556.

17. Szymczak AL, Workman CJ, Wang Y, et al. Correction of multi-gene deficiency in vivo using a single 'self-cleaving' 2A peptide-based retroviral vector. Nature biotechnology. 2004;22(5):589-594.

18. Osborn MJ, Panoskaltsis-Mortari A, McElmurry RT, et al. A picornaviral 2A-like sequence-based tricistronic vector allowing for high-level therapeutic gene expression coupled to a dual-reporter system. Molecular therapy : the journal of the American Society of Gene Therapy. 2005;12(3):569-574.

19. Hu T, Fu Q, Chen P, Zhang K, Guo D. Generation of a stable mammalian cell line for simultaneous expression of multiple genes by using 2A peptide-based lentiviral vector. Biotechnology letters. 2009;31(3):353-359.

20. Lengler J, Holzmuller H, Salmons B, Gunzburg WH, Renner M. FMDV-2A sequence and protein arrangement contribute to functionality of CYP2B1-reporter fusion protein. Analytical biochemistry. 2005;343(1):116-124.

21. Funston GM, Kallioinen SE, de Felipe P, Ryan MD, Iggo RD. Expression of heterologous genes in oncolytic adenoviruses using picornaviral 2A sequences that trigger ribosome skipping. The Journal of general virology. 2008;89(Pt

2):389-396.

22. Rothwell DG, Crossley R, Bridgeman JS, et al. Functional expression of secreted proteins from a bicistronic retroviral cassette based on foot-and-mouth disease virus 2A can be position dependent. Human gene therapy. 2010;21(11):1631-1637.

23. Yeom HJ, Koo OJ, Yang J, et al. Generation and characterization of human heme oxygenase-1 transgenic pigs. PloS one. 2012;7(10):e46646.

24. He L, Hannon GJ. MicroRNAs: small RNAs with a big role in gene regulation. Nature reviews. Genetics. 2004;5(7):522-531.

25. Pillai RS, Bhattacharyya SN, Filipowicz W. Repression of protein synthesis by miRNAs: how many mechanisms? Trends in cell biology. 2007;17(3):118-126.

26. Carey BW, Markoulaki S, Hanna J, et al. Reprogramming of murine and human somatic cells using a single polycistronic vector. Proceedings of the National Academy of Sciences of the United States of America. 2009;106(1):157-162.

27. Chang CW, Lai YS, Pawlik KM, et al. Polycistronic lentiviral vector for "hit and run" reprogramming of adult skin fibroblasts to induced pluripotent stem cells. Stem cells (Dayton, Ohio). 2009;27(5):1042-1049.

28. Kaji K, Norrby K, Paca A, Mileikovsky M, Mohseni P, Woltjen K. Virus-free induction of pluripotency and subsequent excision of reprogramming factors. Nature. 2009;458(7239):771-775.

29. Fang J, Qian JJ, Yi S, et al. Stable antibody expression at therapeutic levels using the 2A peptide. Nature biotechnology. 2005;23(5):584-590.

30. Trichas G, Begbie J, Srinivas S. Use of the viral 2A peptide for bicistronic expression in transgenic mice. BMC biology. 2008;6:40.

31. Chan HY, V S, Xing X, et al. Comparison of IRES and F2A-based locus-specific multicistronic expression in stable mouse lines. PloS one. 2011;6(12):e28885.

32. Yang D, Wang CE, Zhao B, et al. Expression of Huntington's disease protein results in apoptotic neurons in the brains of cloned transgenic pigs. Human molecular genetics. 2010;19(20):3983-3994.

33. Deng W, Yang D, Zhao B, et al. Use of the 2A peptide for generation of multi-transgenic pigs through a single round of nuclear transfer. PloS one. 2011;6(5):e19986.

34. Kues WA, Schwinzer R, Wirth D, et al. Epigenetic silencing and tissue independent expression of a novel tetracycline inducible system in double-transgenic pigs. FASEB journal : official publication of the Federation of American Societies for Experimental Biology. 2006;20(8):1200-1202.

35. Hasegawa K, Cowan AB, Nakatsuji N, Suemori H. Efficient multicistronic expression of a transgene in human embryonic stem cells. Stem cells (Dayton, Ohio). 2007;25(7):1707-1712.

36. Fisicaro N, Londrigan SL, Brady JL, et al. Versatile co-expression of graft-protective proteins using 2A-linked cassettes. Xenotransplantation.

2011;18(2):121-130.

37. Nakayama K. Furin: a mammalian subtilisin/Kex2p-like endoprotease involved in processing of a wide variety of precursor proteins. The Biochemical journal. 1997;327 (Pt 3):625-635.

38. Martoglio B, Dobberstein B. Signal sequences: more than just greasy peptides. Trends in cell biology. 1998;8(10):410-415.

39. de Felipe P, Ryan MD. Targeting of proteins derived from self-processing polyproteins containing multiple signal sequences. Traffic (Copenhagen, Denmark). 2004;5(8):616-626.

40. Donnelly ML, Luke G, Mehrotra A, et al. Analysis of the aphthovirus 2A/2B polyprotein 'cleavage' mechanism indicates not a proteolytic reaction, but a novel translational effect: a putative ribosomal 'skip'. The Journal of general virology. 2001;82(Pt 5):1013-1025.

41. Brown BD, Venneri MA, Zingale A, Sergi Sergi L, Naldini L. Endogenous microRNA regulation suppresses transgene expression in hematopoietic lineages and enables stable gene transfer. Nature medicine. 2006;12(5):585-591.

42. Bartel DP. MicroRNAs: target recognition and regulatory functions. Cell. 2009;136(2):215-233.

43. Tay Y, Zhang J, Thomson AM, Lim B, Rigoutsos I. MicroRNAs to Nanog, Oct4 and Sox2 coding regions modulate embryonic stem cell differentiation. Nature. 2008;455(7216):1124-1128.

Chapter II

Human preformed antibody response to α1,3Gal and Neu5Gc antigen

Reprinted or edited from

Xenotransplantation. 2016;23(4):279-92.

Introduction

Allotransplantation is the most effective treatment for end-stage organ failure; however, there is a severe worldwide shortage of organ donors. To address this issue, xenotransplantation using pig organs could be considered. However, there are a number of obstacles that need to be overcome for pig-to-primate xenotransplantation to be successful, in particular the presence of preformed antibodies against porcine-specific glycoconjugates [1, 2]. Heart or kidney xenotransplants from α1,3-galactosyl transferase-knockout (GT-KO) pigs into baboons revealed that graft rejections were mediated by antibodies that bound to non-Gal antigens and complement activation [3, 4]. These findings indicate that some porcine antigens remain and are reactive in primates, despite the absence of α1,3Gal antigen [5-9].

Sialic acid is a family of nine-carbon acidic monosaccharides typically located at the termini of carbohydrate chains of glycoconjugates [10], and are crucial for certain molecular and cellular interactions [11]. N-acetylneuraminic acid (Neu5Ac) and N-glycolylneuraminic acid (Neu5Gc) are the most abundant sialic acids in mammals. The biosynthesis of Neu5Gc is mediated by cytidine monophosphate (CMP)-N-acetylneuraminic acid hydroxylase (CMAH), which is responsible for converting CMP-Neu5Ac to CMP-Neu5Gc [12]. The CMAH gene is functional in all mammals, including nonhuman primates, with the distinct exception of humans. Therefore, endogenous Neu5Gc is absent in humans, and they retain natural xenoreactive antibodies against Neu5Gc [13, 14]. However, the impact of anti-Neu5Gc antibody in xenotransplantation remains unknown because anti-Neu5Gc antibody is not produced by nonhuman primates

used in pig-to-nonhuman primate xenotransplantation.

Previous studies have shown that antibodies against Neu5Gc are present in human sera [15-19]. However, the dominant antibody isotype were quite different in each study and function related to complement activation by these antibodies using a large number of human sera are yet to be fully elucidated [15-19]. In addition, the majority of these studies to date have used porcine cells, which express additional antigens that can be targeted by humans, complicating their interpretations [15-17].

To investigate the antibody reactivity to the Neu5Gc and α1,3Gal antigens by humans, I generated human embryonic kidney 293 (HEK293) cells that stably express Neu5Gc or α1,3Gal and determined the antibody isotypes, relative concentrations and their ability to induce complement-dependent cytotoxicity (CDC) to these two carbohydrate targets in the serum of 100 healthy individuals.

Materials and Methods

Cells and culture

HEK293 cells (CRL-1573, ATCC, VA, USA) derived from the kidney of an aborted human embryo were purchased. HEK293 cells expressing porcine GT (HEK293-pGT) or porcine CMAH (HEK293-pCMAH) were generated by transfecting HEK293 with pGT/pcDNA3.1 or pCMAH/pCMV-Tag3, respectively, and following selection with G418 sulfate (AG Scientific Inc, CA, USA). The MPN3 cell line was generated as previously reported [20]. Briefly, isolated primary pig aortic endothelial cells (PAECs) were obtained from fresh aortas of Minnesota miniature pigs maintained at Finch University of Health Sciences/Chicago Medical School (North Chicago, IL, USA) and stably introduced with the pRNS-1 plasmid containing the gene encoding the SV40 large T antigen (SV40T/pRNS-1). GTKO PAECs were kindly provided by Dr. Peter Cowan (Immunology Research Centre, St Vincent's Hospital Melbourne, Australia). The immortalized GTKO PAEC line (GTKO PAECL) was generated by stable introduction of the SV40T/pRNS-1. All cell lines were maintained in Dulbecco's modified Eagle's medium (DMEM; WelGENE, Daegu, Korea) supplemented with 10% (v/v) fetal bovine serum (FBS; Gibco, MD, USA) and 1% (v/v) antibiotic-antimycotic solution (Gibco, MD, USA), and incubated at 37°C/5% CO2. The FBS used throughout this study was derived from a single bottle to maintain consistent Neu5Gc background levels.

Plasmids

The sequences of genes encoding porcine GT and CMAH were obtained from cDNA derived from MPN3 cells. The porcine GT or CMAH sequences were inserted into pcDNA3.1 or pCMV-Tag3, respectively. I used oligonucleotide primers that were specific for porcine GT (5′-ATG AAT GTC AAA GGA AGA GTG-3′ and 5′-TCA GAT GTT ATT TCT AAC C-3′) and CMAH (5′-ATG AGC AGC ATC GAA CAA ACG-3′ and 5′-CTA CCC AGA GCA CAT CAG G-3′).

Western blotting

Western blot was performed using appropriate primary and secondary antibodies. The following primary antibodies were used: mouse anti-Xpress™ (1:5000; Invitrogen, CA, USA); mouse anti-Myc-Tag (1:2000; Cell Signaling, MA, USA); and mouse anti-alpha tubulin (1:5000; AbFrontier, Seoul, Korea). I used a horseradish peroxidase (HRP)-conjugated goat anti-mouse IgG (1:10000; AbFrontier, Seoul, Korea) as a secondary antibody. Chemiluminescent detection was conducted using the AbSignal™ Kit (AbClon, Seoul, Korea).

Flow cytometry

To detect α1,3Gal, I used 1 μg/mL fluorescein isothiocyanate (FITC)-conjugated Bandeiraea simplicifolia isolectin B4 (BS-IB4; Sigma Aldrich, MO, USA). To detect Neu5Gc, detached cells were stained with chicken anti-Neu5Gc or chicken IgY isotype control diluted 1:200 in 1X Neu5Gc assay blocking solution (all from

BioLegend, CA, USA), followed by FITC-conjugated anti-chicken IgY (1:200, Jackson ImmunoResearch, PA, USA). To detect the binding of human preformed antibodies, 2 × 105 cells were incubated with 30% heat-inactivated serum samples diluted in 1X Neu5Gc assay blocking solution for 30 min. FITC-conjugated anti-human IgM, IgG (Sigma Aldrich, MO, USA) were used as a secondary antibody.

To determine the degree of CDC, 2 × 105 cells were incubated with 30% serum samples diluted in 1X Neu5Gc assay blocking solution at room temperature (RT) for 60 min for the CDC experiment except for figure 6I and 6J. Meanwhile, 2 × 105 cells were incubated with 30% heat-inactivated serum (HIS) or 30% IgG-depleted serum (GDS; see section IgG depletion of serum samples in Materials and Methods) from samples in the IgG^{high} group (see section Effect of IgG depletion on CDC for α1,3Gal and Neu5Gc in Results) at RT for 30 min. After washing twice with PBS, cells were incubated with 20% rabbit complement (Cedarlane Laboratories, Ontario, Canada) at RT for 30 min for the experiment in figure 6I and 6J. Dead cells were identified by staining with a 7-Aminoactinomycin D (7-AAD; BD Pharmingen, CA, USA). Stained cells were analyzed using a BD FACSCalibur (BD Biosciences, CA, USA).

Preparation of human serum samples

Blood samples from total 120 healthy human donors were collected and the serum separated using protocols approved by the Institutional Review Board of Seoul National University Hospital (IRB #1401-104-549). Blood was collected

into BD Vacutainer® SST tubes (BD Biosciences, CA, USA) and gently inverted five times. Samples were allowed to clot at 4°C for 30 min, and then centrifuged (3000 rpm, 10 min). Collected serum samples were stored at −80°C until required.

IgG depletion of serum samples

An aliquot of each serum sample (400 μL) was incubated at 56°C for 30 min. Serum IgG was depleted by incubating each sample with 200 μL of Protein G Sepharose (GE Healthcare Life Sciences, Uppsala, Sweden) on a rotating platform at RT for 30 min. Samples were then centrifuged (10000 rpm, 5 min) and IgG-depleted sera recovered.

Enzyme-linked immunosorbent assays (ELISAs)

To quantify levels of antibodies against α1,3Gal or Neu5Gc, 96-well Costar 9018 plates (Corning Inc., NY, USA) were coated with 100 μL of Galα1-3Galβ1-4GlcNAcβ-Polyacrylamide (α1,3Gal-PAA), Neu5Gcα-PAA (monosaccharides form), or Control-PAA (each 5 μg/mL; GlycoTech, MD, USA) diluted in 50 mM carbonate-bicarbonate buffer pH 9.6 (Sigma Aldrich, MO, USA) at RT for 2 h. After washing, each 100 μL of serum diluted 1:100 in Tris-buffered saline (TBS) containing 0.1% (v/v) Tween-20 (TBST; Bio-Rad, CA, USA) was added to wells, in triplicate. After washing, each 100 μL of the appropriate secondary antibody diluted 1:5000 in TBST was added to wells. The following secondary antibodies

were used: HRP-conjugated goat anti-human IgM, IgG, IgG1-4 (all from Alpha Diagnostic International, TX, USA). Color was developed using 100 μL of 3,3′,5,5′-Tetramethylbenzidine (Life Technologies, NY, USA). After adding 100 μL of 1 M HCl, the absorbance was measured at 450 nm using a PowerWave HT Microplate Spectrophotometer (BioTek, VT, USA). The values for antibodies against synthetic α1,3Gal or Neu5Gc antigen were calculated by subtracting the absorbance of the wells coated with Control-PAA from that of the wells coated with α1,3Gal-PAA or Neu5Gcα-PAA, respectively.

To determine the degree of complement component 4a (C4a) and complement factor Bb, 2 × 105 cells were incubated with 30% human serum samples at RT for 60 min. Samples were then centrifuged (1500 rpm, 10 min) and each supernatant was harvested. Concentrations of complement component 4a and complement factor Bb of each sample were measured using a BD OptEIA™ human C4a ELISA kit (BD Biosciences, CA, USA) and a MicroVue Bb Plus EIA kit (Quidel Corporation, CA, USA), respectively, according to the manufacturer's protocol.

Statistical analysis

I used GraphPad Prism version 6.0 (GraphPad Software, CA, USA) to conduct statistical analyses. Unpaired or paired t-tests were used to compare results between groups. Analysis of variance (ANOVA) was used to compare results from more than three groups. Pearson correlation analysis and linear regression was used to analyze the correlation between two variables. Results are presented as log2 values of the mean fluorescence intensity (MFI) for antibody binding and

cytotoxicity to fulfill the criteria of normal distribution. P-value less than 0.05 was considered statistically significant.

Results

Expression of α1,3Gal and Neu5Gc in HEK293 cells

To evaluate human antibody reactivity against α1,3Gal and Neu5Gc, I generated plasmid vectors that possessed Xpress-tagged pGT and Myc-tagged pCMAH genes, respectively (Fig. 1A). Following the establishment of HEK293 cells stably expressing the pGT (HEK293-pGT) or pCMAH (HEK293-pCMAH), I confirmed the protein expression of Xpress-pGT and Myc-pCMAH fusion proteins by western blotting (Fig. 1B). In flow cytometric analysis, α1,3Gal was well expressed on the surface of HEK293-pGT cells. It is known that FBS contains high levels of Neu5Gc that can be incorporated into human cells [21, 22]. Hence, above background levels of Neu5Gc were detected on the surface of control HEK293 and HEK293-pGT cells. However, the expression levels of Neu5Gc on HEK293-pCMAH cells were approximately 15-fold higher than on HEK293 and HEK293-pGT cells (Fig. 1C and supplementary Fig. 1).

Antibody binding to HEK293-pGT and HEK293-pCMAH cells

To analyze the binding of human preformed antibodies against α1,3Gal or Neu5Gc, I collected sera from 100 healthy individual donors and evaluated the reactivity by flow cytometry. For HEK293 cells, the mean log2 MFI for IgM and IgG was 3.52 ± 0.81 and 3.28 ± 0.47, respectively. The upper values of IgM and IgG binding, which corresponded to two standard deviations (2SD) above the

mean of controls, were 5.13 and 4.21 respectively.

The mean log2 MFI of IgM for HEK293-pGT cells was significantly increased compared with that for controls (6.27 ± 1.17 vs. 3.52 ± 0.81, $p<0.001$), with 82% of cases exhibiting a log2 MFI more than 2SD greater than the mean of controls. The mean log2 MFI of IgM for HEK293-pCMAH was similar to that for controls (3.55 ± 0.75 vs. 3.52 ± 0.81, $p=0.682$), with only 4% of cases exhibiting a log2 MFI more than 2SD greater than the mean of controls (Fig. 2A).

The mean log2 MFI of IgG for HEK293-pGT cells was significantly higher than that for controls (6.53 ± 1.32 vs. 3.28 ± 0.47, $p<0.001$), with 95% of cases exhibiting a log2 MFI more than 2SD greater than the mean of controls. The mean log2 MFI of IgG for HEK293-pCMAH cells was significantly higher than that controls (4.88 ± 1.46 vs. 3.28 ± 0.47, $p<0.001$), with 62% of cases exhibiting a log2 MFI more than 2SD greater than the mean of controls (Fig. 2A).

I analyzed differences between human preformed antibodies against α1,3Gal and Neu5Gc with respect to ABO blood groups, age, and gender. Individuals belonging to blood group A exhibited a larger amount of IgG for α1,3Gal than those in blood groups B ($p<0.001$), AB ($p<0.001$), and O ($p=0.014$). The log2 MFIs for IgM and IgG against Neu5Gc were not significantly different among blood groups (Fig. 2B). There was no difference in the degree of preformed antibodies against both antigens according to either age or gender (Supplementary Fig. 2A and 2B).

CDC against HEK293-pGT and HEK293-pCMAH cells

I evaluated whether α1,3Gal or Neu5Gc expressed on HEK293 cells were able to induce CDC in response to human sera. In this study, I adopted 30% serum dilution because CDC levels were clearly detected in response with 30% serum samples in a cohort of 10 individuals in my preliminary data (Supplementary Fig. 3). For control HEK293 cells, the mean proportion of cells that were killed by CDC was 6.83 ± 9.88%, with an upper value (2SD) of 26.58%. The basal cytotoxicity level of HEK293 cells in the absence of human serum was 5.20%, indicating that serum-derived Neu5Gc had negligible effect on the CDC assay. The expression of α1,3Gal on HEK293-pGT cells dramatically increased the degree of CDC compared with that for controls (75.44 ± 21.77 vs. 6.83 ± 9.88%, $p<0.0001$), with 93% of human serum samples exhibiting a mean proportion of cytotoxicity more than 2SD greater than the mean for controls (upper quartile, 91.68%; median, 82.50%). The mean proportion of cytotoxicity mediated against HEK293-pGT cells was somewhat higher than that for positive control MPN3 cells (75.44 ± 21.77 vs. 71.14 ± 20.91%, $p=0.004$; Fig. 3A). Correlation analysis showed that the degree of CDC for HEK293-pGT cells positively correlated with that for MPN3 cells ($r2=0.5760$, $p<0.001$; Fig. 3B).

The expression of Neu5Gc on HEK293-pCMAH cells resulted in a greater degree of CDC compared with that seen for controls (25.80 ± 32.25 vs. 6.83 ± 9.88%, $p<0.001$), with 28% of human serum samples exhibiting a mean proportion of cytotoxicity more than 2SD greater than the mean for controls. The degree of CDC was highly variable, with moderate to severe CDC seen in some cases (upper quartile, 45.21%; median, 8.17%). It was also seen for GTKO

PAECL (upper quartile, 34.00%; median, 18.40%). The severity of CDC for HEK293-pCMAH cells was similar to that for positive control GTKO PAECL (25.80 ± 32.25 vs. 26.72 ± 19.43%, p=0.695; Fig. 3A). In correlation analysis, no correlation in CDC was seen between MPN3 and HEK293-pCMAH cells (r2=0.02362, p=0.127). However, a positive correlation was observed between the degree of CDC for HEK293-pCMAH cells and that for GTKO PAECL (r2=0.4715, p<0.001; Fig. 3C). These results suggest that Neu5Gc might actually be a critical antigen among several non-Gal antigens in GTKO pigs.

Ig subtype-specific CDC for α1,3Gal and Neu5Gc

The association between IgM and IgG binding and degree of CDC for HEK293-pGT and HEK293-pCMAH cells was analyzed. The degree of CDC for HEK293-pGT cells positively correlated with log2 MFIs for IgM (r2=0.2144, p<0.001) and IgG (r2=0.1585, p<0.001; Fig. 4A). The degree of CDC for HEK293-pCMAH cells did not correlate with the log2 MFI of IgM (r2=0.03266, p=0.072); however, there was a strong correlation with the log2 MFI of IgG (r2=0.2758, p<0.001; Fig. 4B). In the small cohort of another 20 human subjects, I identified the association between IgM and IgG binding against synthetic α1,3Gal or Neu5Gc antigen and degree of CDC for HEK293-pGT and HEK293-pCMAH, respectively. The degree of CDC for HEK293-pGT significantly correlated with the value for IgM against synthetic α1,3Gal antigen (r2=0.2794, p=0.0166; Supplementary Fig. 4A). However, there was a considerable correlation between the value for IgG against synthetic Neu5Gc antigen and the

degree of CDC for HEK293-pCMAH (r2=0.6877, p<0.001; Supplementary Fig. 4B).

IgG subclass binding for α1,3Gal and Neu5Gc

In humans, four IgG subclasses (IgG1–4) exhibit different complement activation activities [23]. For Ig subclasses analysis, I collected additional fresh human serum samples obtained from 20 healthy blood donors and investigated binding levels of Ig subclasses against each synthetic antigen. The total IgG binding against synthetic α1,3Gal was not associated with IgM binding (p=0.724; data not shown), and the most common subclass of IgG against α1,3Gal was observed to be IgG2 (Fig. 5A). Meanwhile, total IgG binding against synthetic monosaccharide Neu5Gc was not associated with IgM binding (p=0.387; data not shown). The most common subclass of IgG against Neu5Gc was IgG1 (Fig. 5B).

Effect of IgG depletion on CDC for α1,3Gal and Neu5Gc

The actual impact of IgG binding on CDC was investigated using IgG-depleted sera. The 20 serum samples were divided into two groups according to total IgG binding levels for each synthetic antigen in figure 5: IgG^{high} where the optical density 450 (OD 450) was >0.1; and IgG^{low} where the OD 450 was <0.1. There was no significant difference in IgM log2 MFIs between the IgG^{high} and IgG^{low} groups for HEK293-pGT (IgG^{high} vs. IgG^{low}: 0.16 ± 0.15 vs. 0.15 ± 0.18, p=0.891; Fig. 6A) and HEK293-pCMAH cells (IgG^{high} vs. IgG^{low}: 0.07 ± 0.06 vs. 0.03 ±

0.03, p=0.059; Fig. 6B).

Cytotoxicity towards HEK293-pGT cells was significantly higher for the IgG^{high} group than for the IgG^{low} group (88.07 ± 8.97 vs. 64.87 ± 28.00%, p = 0.018). However, I observed greater than 50% cytotoxicity for 77.78% of IgG^{low} group samples (Fig. 6C). For HEK293-pCMAH cells, a considerable degree of CDC was seen for the IgG^{high} group compared with the IgG^{low} group (61.44 ± 25.05 vs. 2.10 ± 1.21%, p < 0.001; Fig. 6D). Following the depletion of IgG, the mean MFI of IgG for HEK293-GT (HIS vs. GDS: 96.32 ± 42.48 vs. 5.45 ± 1.41%, p<0.001; Fig. 6G) and HEK293-pCMAH (HIS vs. GDS: 69.81 ± 27.54 vs. 6.35 ± 1.19%, p<0.001; Fig. 6H) was significantly decreased as a background level, respectively, without any effect on that of IgM for HEK293-pGT (HIS vs. GDS: 102.09 ± 66.69 vs. 105.62 ± 71.21%, p=0.091; Fig. 6E) and HEK293-pCMAH (HIS vs. GDS: 27.47 ± 9.81 vs. 28.72 ± 9.66%, p=0.105; Fig. 6F), respectively. The degree of CDC for HEK293-pGT cells was unchanged (HIS vs. GDS: 73.21 ± 5.81 vs. 76.77 ± 6.61%, p=0.235; Fig. 6I). However, the degree of CDC for HEK293-pCMAH cells was significantly reduced following IgG depletion (HIS vs. GDS: 42.86 ± 16.49 vs. 19.74 ± 8.96%, p<0.001; Fig. 6J).

Activation of complement component 4a (C4a) by α1,3Gal and Neu5Gc

To determine which complement component was activated in response to α1,3Gal and Neu5Gc, I measured levels of complement C4a and factor Bb. The concentration of complement C4a was significantly increased in response to HEK293-pGT cells, compared with that for control HEK293 cells (1.69 ± 0.43 vs.

0.70 ± 0.28, p<0.001). In response to HEK293-pCMAH cells, the concentration of complement C4a was also higher than that for controls (1.09 ± 0.60 vs. 0.70 ± 0.28, p=0.003; Fig. 7A). However, complement factor Bb levels were similar in response to each cell line (HEK293-pGT vs. HEK293: 3.50 ± 0.86 vs. 3.51 ± 0.84, p=0.961; HEK293-pGT vs. HEK293-pCMAH: 3.50 ± 0.86 vs. 3.38 ± 0.84, p=0.063; and HEK293-pCMAH vs. HEK293: 3.38 ± 0.84 vs. 3.51 ± 0.84, p=0.051; Fig. 7B).

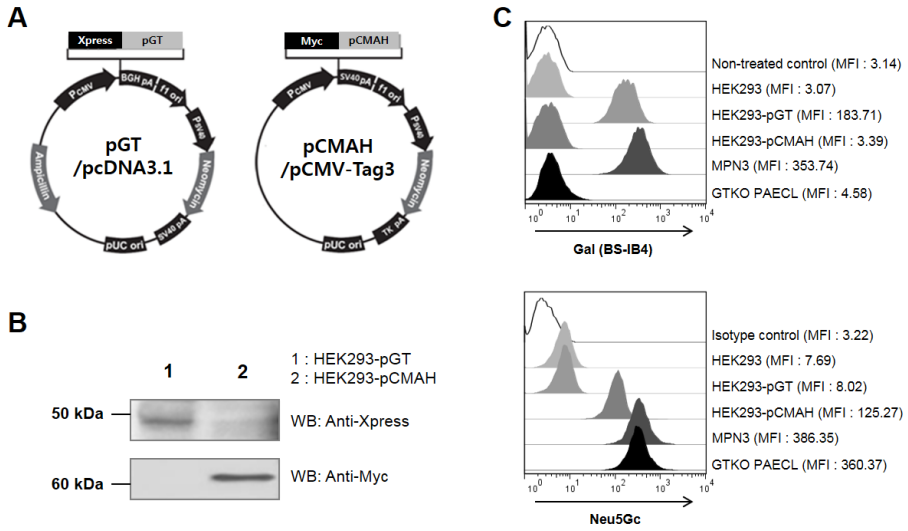

Figure 1. Construction of HEK293 expressing xenogeneic antigen, α1,3Gal or Neu5Gc.

A) Schematic diagram of plasmid vectors for the expression of porcine GT or porcine CMAH. B) The cell lysate of HEK293-pGT or HEK293-pCMAH was subjected to western blotting with either the mouse anti-XpressTM antibody or mouse anti-Myc-Tag antibody, followed by HRP-conjugated goat anti-mouse IgG. C) Cell surface expression of α1,3Gal or Neu5Gc on each cell line was analyzed by flow cytometry. For α1,3Gal detection, each cell line was stained with FITC-conjugated BS-IB4. For Neu5Gc detection, each cell line was incubated with chicken anti-Neu5Gc antibody, followed by FITC-conjugated anti-chicken IgY antibody. MFI, mean fluorescence intensity.

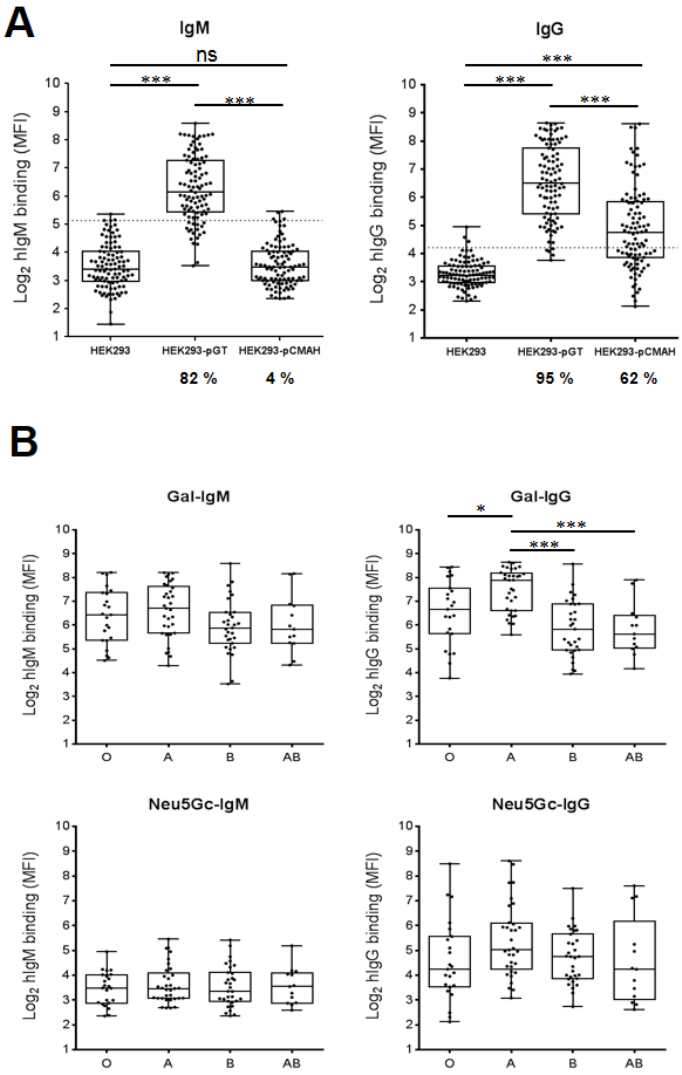

Figure 2. Preformed IgM and IgG binding to xenogeneic antigen, α1,3Gal or Neu5Gc.

A) The binding levels of preformed IgM or IgG to xenogeneic antigen, α1,3Gal or Neu5Gc, were analyzed using flow cytometry. Each cell line was incubated with 30% heat inactivated serum from 100 human subjects, followed by FITC-conjugated anti-human IgM or FITC-conjugated anti-human IgG. Box and

whisker plots are shown with indication of all values. For statistical analysis, paired two-tailed t-test was used to compare results between groups. B) Preformed IgM or IgG binding to each antigen was divided by blood group; O (n=23), A (n=33), B (n=31), and AB (n=13). Box and whisker plots are shown with indication of all values. For statistical analysis, ANOVA was used to compare results among groups.

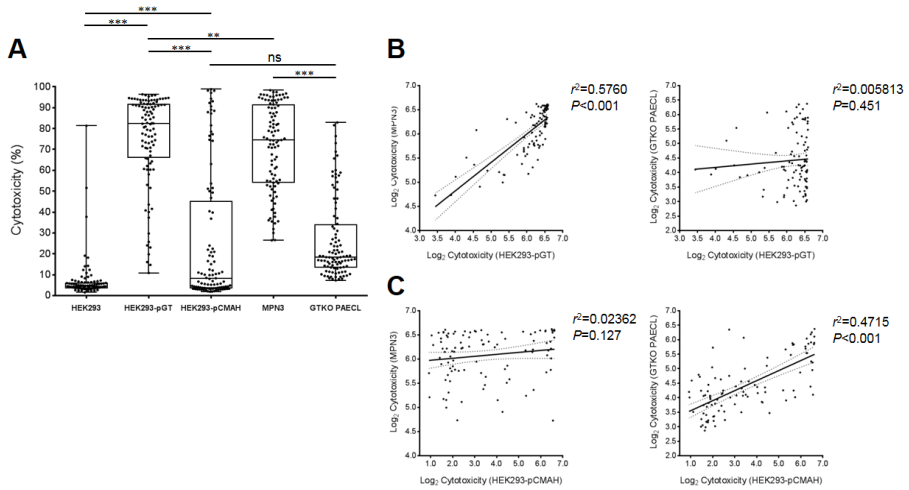

Figure 3. Complement dependent cytotoxicity to each cell line.

A) The levels of complement dependent cytotoxicity to each cell line were analyzed using flow cytometry. Each cell line was incubated with 30% fresh serum from 100 human subjects for 1 hour, followed by 7-AAD staining. Box and whisker plots are shown with indication of all values. For statistical analysis, paired two-tailed t-test was used to compare results between groups. The background CDC levels of each cell line was indicated; HEK293, 5.20; HEK293-pGT, 3.80; HEK293-pCMAH, 4.60; MPN3, 4.80; GTKO PAECL, 5.40. B-C) Correlation analysis in complement dependent cytotoxicity between groups. For statistical analysis, Pearson correlation analysis and linear regression was used to analyze the correlation between two variables.

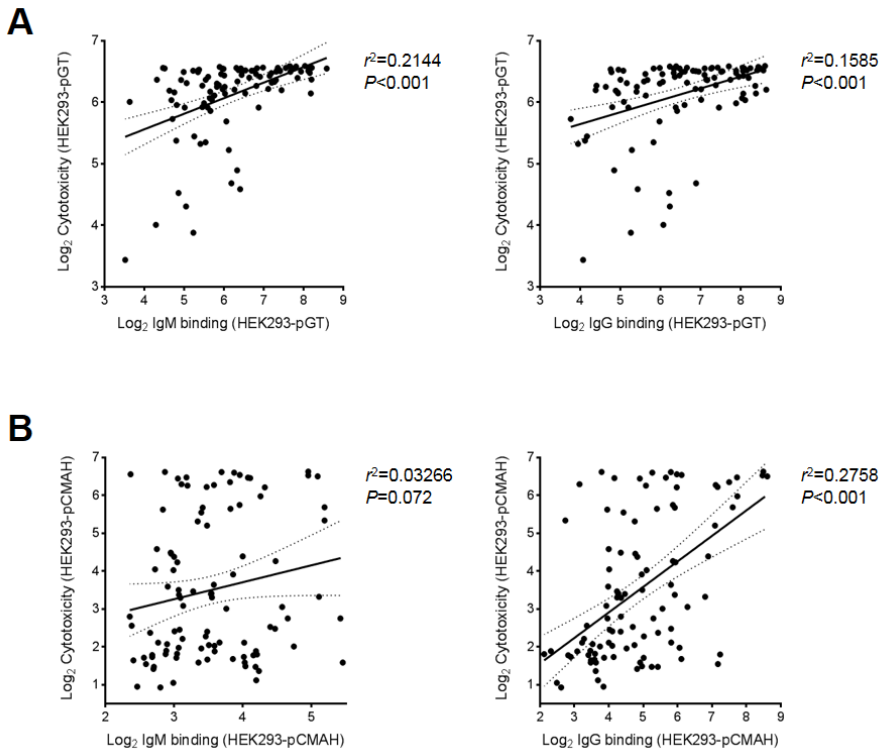

Figure 4. Correlation analysis between preformed antibodies binding and complement dependent cytotoxicity.

A-B) Correlation analysis between preformed antibodies (IgM or IgG) binding and complement dependent cytotoxicity in response to HEK293-pGT (A) or HEK293-pCMAH (B). For statistical analysis, Pearson correlation analysis and linear regression was used to analyze the correlation between two variables.

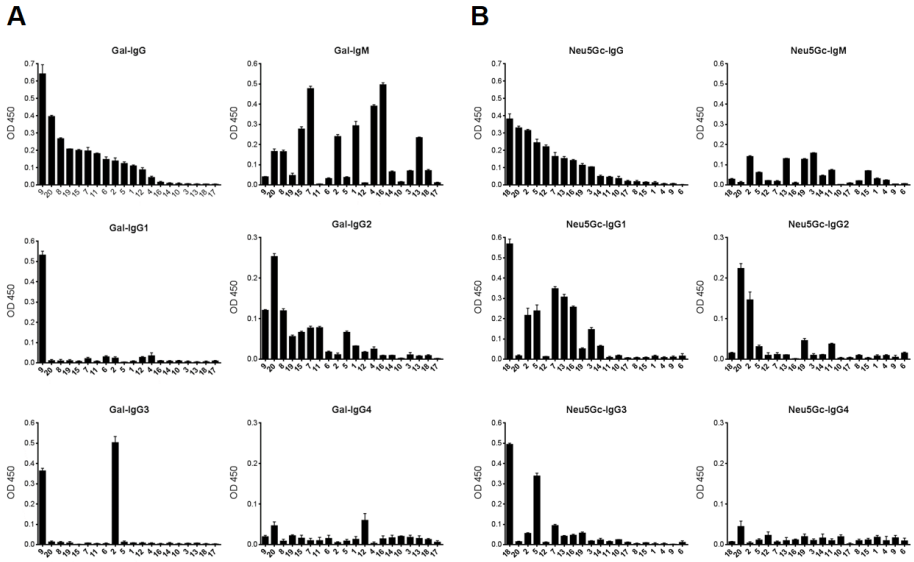

Figure 5. Subclass analysis of preformed IgG against xenogeneic antigen, α1,3Gal or Neu5Gc.

A-B) Using the fresh serum of another 20 human subjects, the levels of preformed IgM, IgG, and IgG subclasses (IgG1, IgG2, IgG3, and IgG4) against α1,3Gal (A) or Neu5Gc (B) were measured by ELISA against α1,3Gal-PAA or Neu5Gcα-PAA, respectively. For the detection of IgG subclasses, HRP-conjugated antibodies to each antigen were used. Bars represent mean absorbance values at OD450 ± SD in each individual. The mean OD450 of each antibody against Control-PAA was indicated; IgM, 0.09 ± 0.05; IgG, 0.09 ± 0.03; IgG1, 0.07 ± 0.02; IgG2, 0.02 ± 0.01; IgG3, 0.05 ± 0.01; IgG4, 0.11 ± 0.05.

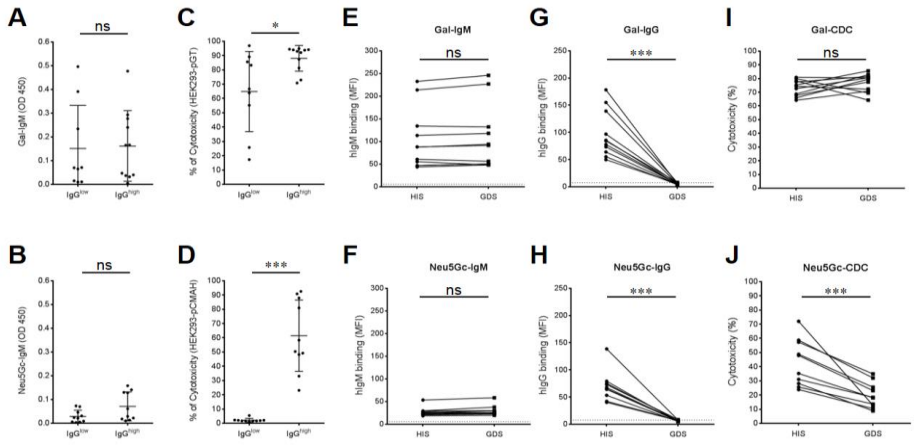

Figure 6. Effect of IgG depletion on complement dependent cytotoxicity.

A-D) Using the fresh serum of 20 human subjects (same samples in figure 5), the levels of preformed IgM and IgG against α1,3Gal or Neu5Gc were measured by ELISA against α1,3Gal-PAA or Neu5Gcα-PAA, respectively. The serum samples were further divided by the level of IgG against α1,3Gal; IgG^{high} (OD>0.1, n=11) and IgG^{low} (OD<0.1, n=9), and that against Neu5Gc; IgG^{high} (OD>0.1, n=10) and IgG^{low} (OD<0.1, n=10) for comparing the IgM levels against each antigen (A and B) and the severity of CDC to each cell line (C and D). Horizontal lines represent mean ± SD for each group. For statistical analysis, unpaired two-tailed t-test was used to compare results between groups. E-J) HEK293-pGT (E, G, and I) or HEK293-pCMAH (F, H, and J) was incubated with 30% heat-inactivated serum (HIS) or 30% IgG-depleted serum (GDS) from each IgG^{high} group for 30 minutes, followed by treatment with FITC-conjugated anti-human IgM (E and F), FITC-conjugated anti-human IgG (G and H), or 20% rabbit complement (I and J) for 30 minutes. The basal MFI of IgM, IgG, and CDC for each cell was indicated using dotted line, respectively. For statistical analysis, paired two-tailed t-test was used to compare results between groups.

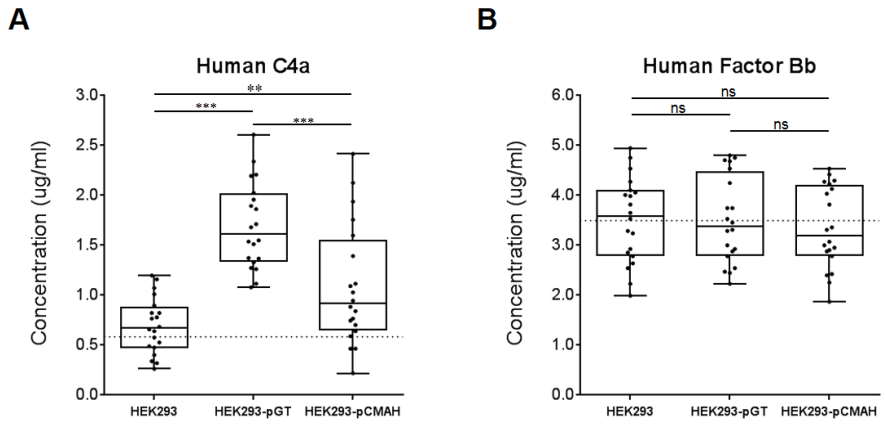

Figure 7. Pathway analysis of complement activation.

A-B) For analyzing the pathway of complement activation, each cell line was incubated with 30% fresh serum from 20 human subjects (same samples in figure 5) for 1 hour. Concentrations of complement component 4a (A) or complement factor Bb (B) of each supernatant were measured by ELISA. Box and whisker plots are shown with indication of all values. Mean basal level of complement component 4a or complement factor Bb from each serum was indicated using dotted line, respectively. For statistical analysis, paired two-tailed t-test was used to compare results between groups.

Discussion

I conducted antibody-binding experiments using HEK293 cells expressing xenogeneic antigens. The results indicated that the majority of human serum samples that I screened contained high levels of IgM and IgG against α1,3Gal. In contrast, partial proportion of the screened samples contained Igs that bound to Neu5Gc, with the dominant isotype found to be IgG. It remains controversial as to whether the antibody response to Neu5Gc is mediated by IgM, IgG, or both Igs. Before obtaining the full coding sequence of porcine CMAH [24, 25], several researchers attempted to determine the level of anti-Neu5Gc antibodies in human sera. Results from two previous studies showed that treatment of porcine red blood cells with neuraminidase resulted in reduced IgG binding to these cells, while IgM binding remained unchanged [15, 16]. However, Saethre et al. showed that IgM and IgG in human serum bound to synthetic Neu5Gc [18]. More recently, Burlak et al. performed crossmatch tests between human serum samples and peripheral blood mononuclear cells from GTKO pigs or GT/CMAH-knockout pigs. They showed that the binding levels of IgM and IgG were significantly decreased following additional deletion in CMAH, with IgG binding reduced to a greater extent than that for IgM [17]. The mechanisms of different activity with respect to human antibody binding remains unclear; however, neighboring glycans or remaining xenoantigens in each cell type likely affect the antibody binding [26].

I found that the degree of preformed IgG against Neu5Gc varied significantly among individuals. Differences in isotypes and the levels of antibodies against each antigen suggested high levels of diversity in the commensal microbiome

expressing the target antigen. The α1,3Gal epitope is expressed within lipopolysaccharides of various Gram-negative bacteria, including Escherichia coli, Klebsiella spp., and Salmonella spp. [27-29]. In addition, the α1,3Gal epitope can also be expressed by some viruses such as human influenza virus and human papillomavirus [30, 31]. High levels of IgM and IgG against α1,3Gal in most human sera could be due to exposure to many microbiomes expressing the α1,3Gal epitope.

To date, there have been no reports of microbiomes directly converting Neu5Ac to Neu5Gc, even though many bacteria can synthesize Neu5Ac [32]. Recently, it was shown that exogenous Neu5Gc can be incorporated and expressed on surface lipooligosaccharides of nontypeable Haemophilus influenzae (NTHi), a human specific Gram-negative bacterium [33]. NTHi is an opportunistic pathogen that can cause respiratory infection, with highest incidence in children younger than 12 months, and in the elderly [34, 35]. Opportunistic and temporary exposure to NTHi might induce the production of Anti-Neu5Gc antibodies. Similar to NTHi, it was previously reported that dietary Neu5Gc can be incorporated in human cells. However, Tahara et al. [36] showed that intraperitoneal (ip) injection of syngeneic Neu5Gc-expressing cells failed in induction of anti-Neu5Gc Abs in CMAH-/- mice. In another study, the feeding of several Neu5Gc-containing materials also failed in generation of anti-Neu5Gc Abs in CMAH-/- mice reared in SPF facility [33]. As our knowledge, the ideal pathway for the anti-Neu5Gc Abs production in humans seems to be originated from the exposure of Neu5Gc-expressing microbiome.

In this study, the degree of binding for IgGs against α1,3Gal were significantly

lower for cases in blood groups B and AB compared with those in blood group A. This phenomenon was previously observed by other research groups [37, 38]. It is possible that this is due to structural similarities between α1,3Gal and group B epitopes. The only structural difference between these epitopes is that the blood group B epitope has a fucose-linked α1,2 to the penultimate galactose. There was no difference in antibody-binding levels against Neu5Gc among ABO blood groups.

In this study, I performed CDC assay at room temperature to replicate the protocols for the clinical crossmatch test [39-41]. In addition, a recent study showed that incubation at room temperature can be useful for investigating the degree of antibody-mediated CDC [42]. I identified that the binding of antibodies to xenoantigens, either α1,3Gal or Neu5Gc, on HEK293 cells caused CDC. Similar to the antibody-binding degree, CDC of HEK293-pGT cells was apparent for the majority of screened human serum samples. The antibody binding levels for IgM and IgG positively correlated with the degree of CDC for HEK293-pGT cells. For HEK293-pCMAH cells, however, a low proportion of serum samples induced CDC. In correlation analysis, only IgG binding positively correlating with the degree of CDC for HEK293-pCMAH cells. Actually, the degree of CDC was significantly reduced when cells were incubated with IgG-depleted sera. I found that IgG1 was the most common subclass that could strongly activate the complement response. These data indicate that IgG binding to Neu5Gc is required to induce CDC. I also investigated the levels of two typical complement components, C4a and factor Bb, using human serum samples. In binding to α1,3Gal and Neu5Gc, the level of C4a was distinctly increased, but there was no

significant change in the factor Bb level. However, this observation was not able to thoroughly exclude the possibility of complement activation via the lectin pathway.

Recently, CMAH knockout mice [43] and CMAH knockout pigs [44] have been generated. Tahara et al. showed that pancreatic islets from wild-type (WT) C57BL/6 mice transplanted into syngeneic CMAH-knockout mice were rejected. However, transplanted WT hearts were not rejected in syngeneic CMAH-knockout mice, even though the recipient CMAH-knockout mice had high levels of antibodies against Neu5Gc [36]. In this model, the different responses observed for islet and heart transplantation could be attributed to discrepancies in Neu5Gc expression between the two tissues. Results from another study revealed that Neu5Gc expression levels for mouse endothelial cells were much lower than those for porcine or bovine endothelial cells [45]. There are considerable differences in the expression of Neu5Gc across pig cells and tissues [25, 45]. It is clear that Neu5Gc is highly expressed on the surface of endothelial cells and pancreatic islet cells [45-47].

In this current study, Neu5Gc on HEK293 cells sufficiently induced IgG binding and CDC in response to some of the serum samples that were screened. I also identified certain serum samples that induced considerable CDC in response to GTKO PAECL. I also found that there was a significant positive correlation between the degree of CDC to HEK293-pCMAH cells and that to GTKO PAECL. These results suggested that porcine Neu5Gc might be a critical antigen among those that participate in the rejection of porcine xenografts in humans.

In the current study, I induced expression of xenogeneic Neu5Gc in human cells to examine the degree of human antibody binding and CDC to this antigen. Although the Neu5Gc expression levels on control HEK293 and HEK293-pGT cells were quite lower than those on HEK293-pCMAH, there were some FBS-derived Neu5Gc expression on these cells and this might interfere with the precise investigation of both antibody binding and CDC against Neu5Gc and α1,3Gal antigen. In addition, the binding mechanism of antibodies to carbohydrate antigens is still unclear. It is previously reported that there are various types of Neu5Gc-containing epitopes in mammalian cells and anti-Neu5Gc antibodies have different reactivity against each Neu5Gc-containing epitope [48, 49]. Therefore, it is also possible that differences in neighboring carbohydrate residues between humans and pigs could influence antibody binding against Neu5Gc, even though HEK293 cells have been previously used in some antigenicity studies [9, 50]. Additionally, I collected human serum samples from a Korean population. To the best of our knowledge, although there is a report showing anti-Gal and anti-non-Gal antibody levels in sera from human subjects from different geographic regions [51], there has been no report for regional differences in the levels of antibodies against Neu5Gc. However, the differences in quantity and isotype of antibodies against Neu5Gc in each study might be originated from regional differences because it was previously reported that there are a differences in the composition of the human gut microbiome based on geography [52, 53], even though it has not been widely investigated whether which microbiome can induce the production of antibodies against Neu5Gc in humans.

Despite the limitations mentioned above, use of the HEK293 cell line clearly demonstrated differences in human antibody binding and subsequent cytotoxicity between α1,3Gal and Neu5Gc. The overall levels of antibody binding and CDC for Neu5Gc were relatively low compared with those for α1,3Gal. Some of the serum samples contained high levels of preformed anti-Neu5Gc IgGs, and induced severe CDC in HEK293 cells expressing Neu5Gc. I also observed that GTKO PAECL expressed considerable levels of Neu5Gc on the surface of cells. These were able to induce severe antibody-mediated CDC for serum samples that contained high levels of Anti-Neu5Gc IgGs. Therefore, these results suggest that additional knockout of CMAH gene in GTKO in combination with human complement regulatory protein(s) transgenic pigs will be required for clinical xenotransplantation.

References

1. Cascalho M, Platt JL. The immunological barrier to xenotransplantation. Immunity. 2001;14(4):437-446.

2. Joziasse DH, Oriol R. Xenotransplantation: the importance of the Galalpha1,3Gal epitope in hyperacute vascular rejection. Biochimica et biophysica acta. 1999;1455(2-3):403-418.

3. Kuwaki K, Tseng YL, Dor FJ, et al. Heart transplantation in baboons using alpha1,3-galactosyltransferase gene-knockout pigs as donors: initial experience. Nat Med. 2005;11(1):29-31.

4. Chen G, Qian H, Starzl T, et al. Acute rejection is associated with antibodies to non-Gal antigens in baboons using Gal-knockout pig kidneys. Nat Med. 2005;11(12):1295-1298.

5. Ezzelarab M, Ayares D, Cooper DK. Carbohydrates in xenotransplantation. Immunol Cell Biol. 2005;83(4):396-404.

6. Yeh P, Ezzelarab M, Bovin N, et al. Investigation of potential carbohydrate antigen targets for human and baboon antibodies. Xenotransplantation. 2010;17(3):197-206.

7. Miyagawa S, Ueno T, Nagashima H, Takama Y, Fukuzawa M. Carbohydrate antigens. Curr Opin Organ Transplant. 2012;17(2):174-179.

8. Burlak C, Wang ZY, Chihara RK, et al. Identification of human preformed antibody targets in GTKO pigs. Xenotransplantation. 2012;19(2):92-101.

9. Byrne GW, Stalboerger PG, Du Z, Davis TR, McGregor CG. Identification of new carbohydrate and membrane protein antigens in cardiac xenotransplantation. Transplantation. 2011;91(3):287-292.

10. Traving C, Schauer R. Structure, function and metabolism of sialic acids. Cell Mol Life Sci. 1998;54(12):1330-1349.

11. Schauer R. Sialic acids as regulators of molecular and cellular interactions. Curr Opin Struct Biol. 2009;19(5):507-514.

12. Kawano T, Koyama S, Takematsu H, et al. Molecular cloning of cytidine monophospho-N-acetylneuraminic acid hydroxylase. Regulation of species- and tissue-specific expression of N-glycolylneuraminic acid. J Biol Chem. 1995;270(27):16458-16463.

13. Irie A, Koyama S, Kozutsumi Y, Kawasaki T, Suzuki A. The molecular basis for the absence of N-glycolylneuraminic acid in humans. J Biol Chem. 1998;273(25):15866-15871.

14. Chou HH, Takematsu H, Diaz S, et al. A mutation in human CMP-sialic acid hydroxylase occurred after the Homo-Pan divergence. Proc Natl Acad Sci U S A. 1998;95(20):11751-11756.

15. Zhu A, Hurst R. Anti-N-glycolylneuraminic acid antibodies identified in healthy human serum. Xenotransplantation. 2002;9(6):376-381.

16. Miwa Y, Kobayashi T, Nagasaka T, et al. Are N-glycolylneuraminic acid (Hanganutziu-Deicher) antigens important in pig-to-human xenotransplantation? Xenotransplantation. 2004;11(3):247-253.

17. Burlak C, Paris LL, Lutz AJ, et al. Reduced binding of human antibodies to cells from GGTA1/CMAH KO pigs. American journal of transplantation : official journal of the American Society of Transplantation and the American Society of Transplant Surgeons. 2014;14(8):1895-1900.

18. Saethre M, Baumann BC, Fung M, Seebach JD, Mollnes TE. Characterization of natural human anti-non-gal antibodies and their effect on activation of porcine gal-deficient endothelial cells. Transplantation. 2007;84(2):244-250.

19. Nguyen DH, Tangvoranuntakul P, Varki A. Effects of natural human antibodies against a nonhuman sialic acid that metabolically incorporates into activated and malignant immune cells. Journal of immunology (Baltimore, Md. : 1950). 2005;175(1):228-236.

20. Kim D, Kim JY, Koh HS, et al. Establishment and characterization of endothelial cell lines from the aorta of miniature pig for the study of xenotransplantation. Cell Biol Int. 2005;29(8):638-646.

21. Tangvoranuntakul P, Gagneux P, Diaz S, et al. Human uptake and incorporation of an immunogenic nonhuman dietary sialic acid. Proceedings of the National Academy of Sciences of the United States of America. 2003;100(21):12045-12050.

22. Bardor M, Nguyen DH, Diaz S, Varki A. Mechanism of uptake and incorporation of the non-human sialic acid N-glycolylneuraminic acid into human cells. The Journal of biological chemistry. 2005;280(6):4228-4237.

23. Kaul M, Loos M. Dissection of C1q capability of interacting with IgG. Time-dependent formation of a tight and only partly reversible association. J Biol Chem. 1997;272(52):33234-33244.

24. Schlenzka W, Shaw L, Kelm S, et al. CMP-N-acetylneuraminic acid hydroxylase: the first cytosolic Rieske iron-sulphur protein to be described in Eukarya. FEBS Lett. 1996;385(3):197-200.

25. Song KH, Kang YJ, Jin UH, et al. Cloning and functional characterization of pig CMP-N-acetylneuraminic acid hydroxylase for the synthesis of N-glycolylneuraminic acid as the xenoantigenic determinant in pig-human xenotransplantation. Biochem J. 2010;427(1):179-188.

26. Liang CH, Wang SK, Lin CW, Wang CC, Wong CH, Wu CY. Effects of neighboring glycans on antibody-carbohydrate interaction. Angewandte Chemie (International ed. in English). 2011;50(7):1608-1612.

27. Bjorndal H, Lindberg B, Nimmich W. Structural studies on Klebsiella O groups 1 and 6 lipopolysaccharides. Acta chemica Scandinavica. 1971;25(2):750.

28. Jansson PE, Lindberg AA, Lindberg B, Wollin R. Structural studies on the hexose region of the core in lipopolysaccharides from Enterobacteriaceae. European journal of biochemistry / FEBS. 1981;115(3):571-577.

29. Galili U, Mandrell RE, Hamadeh RM, Shohet SB, Griffiss JM. Interaction between human natural anti-alpha-galactosyl immunoglobulin G and bacteria of the human flora. Infection and immunity. 1988;56(7):1730-1737.

30. Galili U, Repik PM, Anaraki F, Mozdzanowska K, Washko G, Gerhard W. Enhancement of antigen presentation of influenza virus hemagglutinin by the natural human anti-Gal antibody. Vaccine. 1996;14(4):321-328.

31. Tremont-Lukats IW, Avila JL, Tapia F, Hernandez D, Caceres-Dittmar G, Rojas M. Abnormal expression of galactosyl(alpha 1-->3) galactose epitopes in squamous cells of the uterine cervix infected by human papillomavirus. Pathobiology : journal of immunopathology, molecular and cellular biology. 1996;64(5):239-246.

32. Vimr ER, Kalivoda KA, Deszo EL, Steenbergen SM. Diversity of microbial sialic acid metabolism. Microbiol Mol Biol Rev. 2004;68(1):132-153.

33. Taylor RE, Gregg CJ, Padler-Karavani V, et al. Novel mechanism for the generation of human xeno-autoantibodies against the nonhuman sialic acid N-glycolylneuraminic acid. The Journal of experimental medicine. 2010;207(8):1637-1646.

34. Agrawal A, Murphy TF. Haemophilus influenzae infections in the H. influenzae type b conjugate vaccine era. J Clin Microbiol. 2011;49(11):3728-3732.

35. Erwin AL, Smith AL. Nontypeable Haemophilus influenzae: understanding virulence and commensal behavior. Trends Microbiol. 2007;15(8):355-362.

36. Tahara H, Ide K, Basnet NB, et al. Immunological property of antibodies against N-glycolylneuraminic acid epitopes in cytidine monophospho-N-acetylneuraminic acid hydroxylase-deficient mice. Journal of immunology

(Baltimore, Md. : 1950). 2010;184(6):3269-3275.

37. Galili U, Buehler J, Shohet SB, Macher BA. The human natural anti-Gal IgG. III. The subtlety of immune tolerance in man as demonstrated by crossreactivity between natural anti-Gal and anti-B antibodies. The Journal of experimental medicine. 1987;165(3):693-704.

38. McMorrow IM, Comrack CA, Nazarey PP, Sachs DH, DerSimonian H. Relationship between ABO blood group and levels of Gal alpha,3Galactose-reactive human immunoglobulin G. Transplantation. 1997;64(3):546-549.

39. Pena JR, Fitzpatrick D, Saidman SL. Complement-dependent cytotoxicity crossmatch. Methods in molecular biology (Clifton, N.J.). 2013;1034:257-283.

40. Bray RA. Lymphocyte crossmatching by flow cytometry. Methods in molecular biology (Clifton, N.J.). 2013;1034:285-296.

41. Jackson AM, Lucas DP, Badders JL. A flow cytometric crossmatch test using endothelial precursor cells isolated from peripheral blood. Methods in molecular biology (Clifton, N.J.). 2013;1034:319-329.

42. Shah TA, Mauriello CT, Hair PS, et al. Clinical hypothermia temperatures increase complement activation and cell destruction via the classical pathway. Journal of translational medicine. 2014;12:181.

43. Hedlund M, Tangvoranuntakul P, Takematsu H, et al. N-glycolylneuraminic acid deficiency in mice: implications for human biology and evolution. Mol Cell Biol. 2007;27(12):4340-4346.

44. Kwon DN, Lee K, Kang MJ, et al. Production of biallelic CMP-Neu5Ac hydroxylase knock-out pigs. Sci Rep. 2013;3:1981.

45. Morozumi K, Kobayashi T, Usami T, et al. Significance of histochemical expression of Hanganutziu-Deicher antigens in pig, baboon and human tissues. Transplant Proc. 1999;31(1-2):942-944.

46. Komoda H, Miyagawa S, Kubo T, et al. A study of the xenoantigenicity of adult pig islets cells. Xenotransplantation. 2004;11(3):237-246.

47. Kim YG, Harvey DJ, Yang YH, Park CG, Kim BG. Mass spectrometric analysis of the glycosphingolipid-derived glycans from miniature pig endothelial cells and islets: identification of NeuGc epitope in pig islets. J Mass Spectrom. 2009;44(10):1489-1499.

48. Padler-Karavani V, Yu H, Cao H, et al. Diversity in specificity, abundance, and composition of anti-Neu5Gc antibodies in normal humans: potential implications for disease. Glycobiology. 2008;18(10):818-830.

49. Padler-Karavani V, Tremoulet AH, Yu H, Chen X, Burns JC, Varki A. A simple method for assessment of human anti-Neu5Gc antibodies applied to Kawasaki disease. PloS one. 2013;8(3):e58443.

50. Byrne GW, Du Z, Stalboerger P, Kogelberg H, McGregor CG. Cloning and expression of porcine beta1,4 N-acetylgalactosaminyl transferase encoding a new xenoreactive antigen. Xenotransplantation. 2014;21(6):543-554.

51. Kumar G, Satyananda V, Fang J, et al. Is there a correlation between anti-pig antibody levels in humans and geographic location during childhood?

Transplantation. 2013;96(4):387-393.

52. Yatsunenko T, Rey FE, Manary MJ, et al. Human gut microbiome viewed across age and geography. Nature. 2012;486(7402):222-227.

53. Suzuki TA, Worobey M. Geographical variation of human gut microbial composition. Biology letters. 2014;10(2):20131037.

Chapter III

The mechanism of induced anti-glycan antibody production in target glycan-deficient mice

Unpublished results

Introduction

Although clinical transplantation is the most effective treatment for end-stage organ failure, this treatment has a limitation caused by the severe shortage of human organ donation. Glycan-incompatible transplantation such as ABO-incompatible (ABOi) allotransplantation and xenotransplantation have been considered and studied as one of solutions to resolve the limitation. Unfortunately, humans produce antibodies against the carbohydrate antigens, blood group ABO and galactose-α-1,3-galactose (α1,3Gal) antigen, within 6 months after birth [1-3] and these preformed anti-carbohydrate antibodies caused early graft loss if these are not adequately controled [4-7]. Even though hyperacute rejection (HAR) can be prevented by using antibody desensitization protocols [8, 9] and α1,3-galactosyl transferase-knockout (GT-KO) pigs [10, 11], acute and chronic antibody mediated rejection which is induced by de novo synthesized antibodies after transplantation can be an another hurdle.

B cells can be subdivided into B-1 cells, marginal zone (MZ) B cells, and B-2 cells. B-1 cells can be additionally divided into B-1a cells and B-1b cells as per surface expression of CD5 molecule [12, 13]. Among these B cell subpopulations, it is well known that B-2 cells primarily recognize peptide antigens and can be activated with the help of $CD4^+$ T cells and form germinal centers with the help of follicular helper T cells [14]. In contrast, carbohydrate antigens are mainly recognized by B-1 cells and MZ B cells [15, 16]. It is previously reported that some microbial polysaccharides can stimulate B cell receptor (BCR) and toll-like receptors (TLRs) simultaneously (T-independent type 1 response) or induce BCR crosslinking (T-independent type 2 response) and these responses can result in B

cells activation and antibody production against carbohydrate antigens [17].

For glycan-incompatible transplantation situation, it is unknown and need to be addressed that induced anti-carbohydrate antibodies production and underlying mechanism including the questions, so that we can control rejections. However, most of the questions including which B cell subpopulations have specific BCR which can recognize the certain carbohydrate antigens, whether the responses are T cell dependent or independent, and if T cell help is required to the responses, whether T cells can recognize the certain carbohydrate antigens in glycopeptide on major histocompatibility complex (MHC) molecule or in glycolipid on CD1d molecule.

To investigate the questions, I used wild type C57BL/6 (B6) mice and two independent single carbohydrate antigen-deficient mice, which lack the expression of α1,3Gal (B6.GT-/-) or N-glycolylneuraminic acid (Neu5Gc) antigen (B6.CMAH-/-), respectively. I generated human embryonic kidney 293 (HEK293) cells that stably express α1,3Gal, Neu5Gc, or blood group A antigen, respectively. I also generated MILE SVEN 1 (MS1) cells, which is B6 mouse vascular endothelial cells, or MPN3 cells, which is wild type miniature pig aortic endothelial cells, that stable express blood group A antigen, respectively. Using these cells and mice, I established a model for induced anti-carbohydrate antibodies production and investigated that which B cell subsets are reactive for each carbohydrate antigen and T cell help or NK cell help is required for the anti-carbohydrate antibodies production.

Materials and Methods

Cells and culture

HEK293 cells (CRL-1573, ATCC, VA, USA) derived from the kidney of an aborted human embryo and MS1 cells (CRL-2279, ATCC, VA, USA) derived from B6 mouse pancreas endothelium were purchased. The wild type miniature pig aortic endothelial cell line, MPN3, and HEK293 expressing porcine GT (HEK293-pGT) or porcine cytidine monophospho-N-acetylneuraminic acid hydroxylase (CMAH) (HEK293-pCMAH) were generated as previously reported [18, 19]. HEK293 expressing human H-transferase (hHT) and A-transferase (hAT) (HEK293-ATg), MS1-ATg, and MPN3-ATg were generated by transfecting each cells with hHT-T2A-hAT/pCAG1.2, respectively, and following selection with Hygromycin B (Invitrogen, CA, USA). All cell lines were maintained in Dulbecco's modified Eagle's medium (DMEM; WelGENE, Daegu, Korea) supplemented with 10% (v/v) fetal bovine serum (FBS; Gibco, MD, USA) and 1% (v/v) antibiotic-antimycotic solution (Gibco, MD, USA), and incubated at 37°C/5% CO2.

Plasmid

The sequences of genes encoding human HT and AT were obtained from cDNA derived from splenocyte of B6-huHAT(ICAM) transgenic (Tg) mice [20]. The human HT or AT sequences were linked by T2A peptide and inserted into

pCAG1.2 vector (hHT-T2A-hAT/pCAG1.2). I used oligonucleotide primers that were specific for human HT (5′-TTG GTA CCA TGT GGC TCC GGA GCC ATC G-3′ and 5′-CCG AAT TCA GGC TTA GCC AAT GTC CAG AG-3′) and AT (5′-GGA AGC TTA TGG CCG AGG TGT TGC GGA CG-3′ and 5′-ATC TCG AGT CAC GGG TTC CGG ACC GCC TG-3′).

Mice

All mice experiments were approved by the Institutional Animal Care and Use Committee of Seoul National University (IACUC #SNU-150408-2). C57BL/6 (B6), B6.GT-KO (kindly provided by Dr. Peter Cowan, Immunology Research Centre, St Vincent's Hospital Melbourne, Australia) [21], B6.CMAH-KO (kindly provided by Dr. Ajit Varki, University of California, San Diego, CA, USA) [22], B6.GT/CMAH-KO, and B6.ATg (kindly provided by Dr. Peter Cowan, Immunology Research Centre, St Vincent's Hospital Melbourne, Australia) were used. The genotypes and phenotypes were confirmed by polymerase chain reaction (PCR) using genomic deoxyribonucleic acid (gDNA) and flow cytometry using splenocyte of each strain of mice. All mice were maintained in a specific pathogen-free condition at the Biomedical Center for Animal Resource Development of Seoul National University College of Medicine and 10-14 weeks old male mice were used for mice experiments.

Conditioning regimen for mice experiments

Induced antibody production against α1,3Gal, Neu5Gc, and blood group A antigen was elicited by intraperitoneal injection of each indicated mice with 2 × 106 each indicated cells expressing α1,3Gal, Neu5Gc, or blood group A antigen, respectively. The mice were pre-bled on day -4 and immunized twice on day 0 and day 7 and bled on day 21. For the depletion of target cells, the mice were injected intraperitoneally with 200 μg anti-NK1.1 (PK136; Bio X Cell, NH, USA), 200 μg anti-CD4 mAb (GK1.5; Bio X Cell, NH, USA), or 200 μg anti-CD8 (53-6.72; Bio X Cell, NH, USA) twice on day -2 and day 0, respectively. The mice injected intraperitoneally with each isotype-matched antibody were used as controls.

Enzyme-linked immunosorbent assays (ELISAs)

To quantify levels of antibodies against α1,3Gal, Neu5Gc, or blood group A antigen, 96-well Costar 9018 plates (Corning Inc., NY, USA) were coated with 100 μL of Galα1-3Galβ1-4GlcNAcβ-Polyacrylamide (α1,3Gal-PAA), Neu5Gcα-PAA (monosaccharides form), Blood group A-PAA (trisaccharides form; A-PAA), or Control-PAA (each 5 μg/mL; GlycoTech, MD, USA) diluted in 50 mM carbonate-bicarbonate buffer pH 9.6 (Sigma Aldrich, MO, USA) at RT for 2 h. After washing, each 100 μL of serum diluted 1:50 in Tris-buffered saline (TBS) containing 0.1% (v/v) Tween-20 (TBST; Bio-Rad, CA, USA) was added to wells, in triplicate. After washing, each 100 μL of the appropriate secondary antibody diluted 1:3000 in TBST was added to wells. The following secondary antibodies were used: HRP-conjugated goat anti-mouse IgM or IgG, respectively (all from

Sigma Aldrich, MO, USA). After washing, color was developed using 100 μL of 3,3′,5,5′-Tetramethylbenzidine (Life Technologies, NY, USA). After adding 100 μL of 1 M HCl, the absorbance was measured at 450 nm using a PowerWave HT Microplate Spectrophotometer (BioTek, VT, USA). The values for antibodies against synthetic α1,3Gal, Neu5Gc, or blood group A antigen were calculated by subtracting the absorbance of the wells coated with Control-PAA from that of the wells coated with α1,3Gal-PAA, Neu5Gcα-PAA, or A-PAA, respectively.

Flow cytometry

To detect α1,3Gal, I used 1 μg/mL fluorescein isothiocyanate (FITC)-conjugated Bandeiraea simplicifolia isolectin B4 (BS-IB4; Sigma Aldrich, MO, USA). To detect Neu5Gc, detached cells were stained with chicken anti-Neu5Gc or chicken IgY isotype control diluted 1:200 in 1X Neu5Gc assay blocking solution (all from BioLegend, CA, USA), followed by FITC-conjugated anti-chicken IgY (1:200, Jackson ImmunoResearch, PA, USA). To detect blood group A antigen, I used FITC-conjugated mouse anti-human blood group A (NaM87-1F6; BD Pharmingen, CA, USA) or mouse IgG3 isotype control (A112-3; BD Pharmingen, CA, USA).

To analyze B-1a cells and B-1b cells, 5 × 105 peritoneal exudate cells from each mouse were stained with phycoerythrin (PE)-conjugated rat anti-mouse CD19 (1D3), allophycocyanin (APC)-conjugated rat anti-mouse CD11b (M1/70), and PE-cyanine 5 (Cy5)-conjugated rat anti-mouse CD5 (53-7.3). To analyze MZ B cells and B-2 cells, 5 × 105 splenocytes from each mouse were stained with

PE-conjugated rat anti-mouse CD19 (1D3), Alexa Fluor 647 (AF647)-conjugated rat anti-mouse CD23 (B3B4), and Peridinin-Chlorophyll protein (PerCP)-Cy5.5-conjugated rat anti-mouse CD21/CD35 (7G6; all from BD Pharmingen, CA, USA). To analyze BCR specific for each carbohydrate antigen, 5 × 105 mouse cells were additionally stained with PE-Cy7-conjugated rat anti-mouse IgM (R6-60.2; BD Pharmingen, CA, USA) and FITC-conjugated α1,3Gal-PAA, FITC-conjugated Neu5Gcα-PAA, FITC-conjugated A-PAA, or FITC-conjugated Control-PAA (all from GlycoTech, MD, USA).

Statistical analysis

I used GraphPad Prism version 6.0 (GraphPad Software, CA, USA) to conduct statistical analyses. One-way analysis of variance (ANOVA) with multiple comparisons was used to compare results from each group. P-value less than 0.05 was considered statistically significant (*, $p<0.05$; **, $p<0.01$; ***, $p<0.001$). Error bars represent standard deviation (SD) of the mean.

Results

Expression of target antigens in mice and cell lines

To establish a mouse model for induced anti-carbohydrate antibodies production, I adopted target carbohydrate antigen-deficient mice and representative cell lines expressing target carbohydrate antigens, α1,3Gal, Neu5Gc, or blood group A, respectively. Using splenocytes from each group of mice, I confirmed the surface expression of α1,3Gal and Neu5Gc antigen by flow cytometry. The expression of α1,3Gal was not detected in splenocytes from GT-KO or GT/CMAH-KO mice and the splenocytes from CMAH-KO and GT/CMAH-KO mice did not express the Neu5Gc antigens (Fig. 1A). In flow cytometric analysis, the α1,3Gal antigen was well expressed on the surface of MS1, MPN3, and HEK293-pGT and the Neu5Gc was well detected in MS1, MPN3, and HEK293-pCMAH. After generation of stable cell lines expressing blood group A antigen, I identified the strong expression of blood group A antigen on MS1-ATg, MPN3-ATg, and HEK293-ATg, respectively (Fig. 1B).

Induction and characterization of anti-carbohydrate antibodies

To induce antibody production against each carbohydrate antigen, each group of mice were immunized with each HEK293-based indicated cell line twice weekly. After two weeks from second injection, each mouse was bled and the serum samples from each indicated mouse were used for antibody reactivity against

each carbohydrate antigen (Fig. 2A). The serum samples obtained from GT-KO mice immunized with HEK293-pGT had large amount of IgM and IgG against α1,3Gal antigen specifically (Fig. 2B). The considerable amount of IgM and IgG against-Neu5Gc was induced only in CMAH-KO mice immunized with HEK293-pCMAH (Fig. 2C). WT mice immunized with HEK293-ATg successfully produced IgM and IgG against blood group A antigen because WT mice do not express ABO blood group antigen (Fig. 2D). There was no increase of antibody binding to each indicated carbohydrate antigen in the serum samples from WT mice immunized with HEK293. These date sugeested that the induced antibody against each carbohydrate antigen specifically bound to each target antigen without any cross-reactivity to other antigens (Fig. 2B-D).

Analysis of B cell subsets reactive to each carbohydrate antigen in mice peritoneum and spleen

To investigate which B cell subset react to indicated carbohydrate antigen, I isolated B cells from mice peritoneal cavity or spleen and analyzed the binding of synthesized carbohydrate antigens to certain B cell subsets. In flow cytometric analysis, only small proportion of splenic B cells bound to synthesized α1,3Gal or Neu5Gc antigen and the reactive populations were $CD23^{+}$ $CD21^{low}$ B2 cells and $CD23^{-}$ $CD21^{high}$ MZ B cells. There were no distinct populations reactive to synthesized α1,3Gal or Neu5Gc antigen in peritoneal B cells. Otherwise, blood group A antigen-reactive B cells were detected in both spleen and peritoneal cavity. The reactive proportions in peritoneal cavity were much higher than those

in spleen and identified as $CD11b^+$ $CD5^+$ B1a cells and $CD11b^+$ $CD5^-$ B1b cells (Fig. 3A-B).

Effect of T cell subtype depletion on anti-carbohydrate antibodies production

It is unknown whether the production of induced antibody against carbohydrate antigen is T cell-dependent response or not. I adopted T cell subset depletion protocol using depletion antibody against CD4, CD8, and NK1.1, respectively. Each group of mice was intraperitoneally injected with each depletion antibody on day -2 and day 0 and immunized with each cell line on day 0 and day 7. On day 21, each mouse was bled and the serum samples were analyzed (Fig. 4A).

$CD4^+$ T cell depletion caused marked reduction in the production of both IgM and IgG antibodies against carbohydrate antigens. Antibody production to Neu5Gc and blood group A antigen was totally blocked by $CD4^+$ T cell depletion. Although $CD4^+$ T cell depletion also considerably decreased the production of antibody against α1,3Gal antigen, the minimal production of IgM and IgG against α1,3Gal antigen was observed. After the treatment of anti-NK1.1 antibody, the production of IgM and IgG against α1,3Gal and Neu5Gc antigen was decreased. Reduction of target IgG was more marked than IgM in both groups. However, there is no significant difference in levels of IgM and IgG against blood group A antigen by $NK1.1^+$ cell depletion. There was no significant difference in IgM and IgG against α1,3Gal, Neu5Gc, and blood group A antigen by $CD8^+$ T cell depletion. (Fig. 4B-D). Above data showed the critical role of $CD4^+$ T cells in

induced antibody production against each carbohydrate antigen.

Production of anti-carbohydrate antibodies by stimulation with syngeneic or xenogeneic cells

In order to identify whether T cells can recognize carbohydrate portion which is a part of glycopeptide or glycolipid loaded on major histocompatibility complex (MHC) or MHC-like CD1d molecules in response to the indicated carbohydrate antigens in this study, each mouse was immunized with syngeneic MS1 cells or xenogeneic MPN3 cells expressing target carbohydrate antigen (Fig. 5A-B).

IgM and IgG against α1,3Gal were significantly increased in serum samples obtained from GT-KO or GT/CMAH-KO mice immunized with syngeneic MS1 cells. The xenogeneic MPN3 injection provoked larger amount of IgM and IgG production against α1,3Gal in GT-KO or GT/CMAH-KO mice. Similar to induced anti-α1,3Gal antibody production, both IgM and IgG against blood group A were considerably increased in serum samples obtained from WT mice immunized with either syngeneic MS1 or xenogeneic MPN3. However, the amount of IgM and IgG against blood group A was much higher in MS1-injected group than MPN3-injected group. Interestingly, injection of syngeneic MS1 cells did not induce antibody production against Neu5Gc antigen in CMAH-KO or GT/CMAH-KO mice. The production of IgM and IgG against Neu5Gc antigen was significantly observed only in serum samples from CMAH-KO or GT/CMAH-KO mice immunized with xenogeneic MPN3 (Fig. 5C-E).

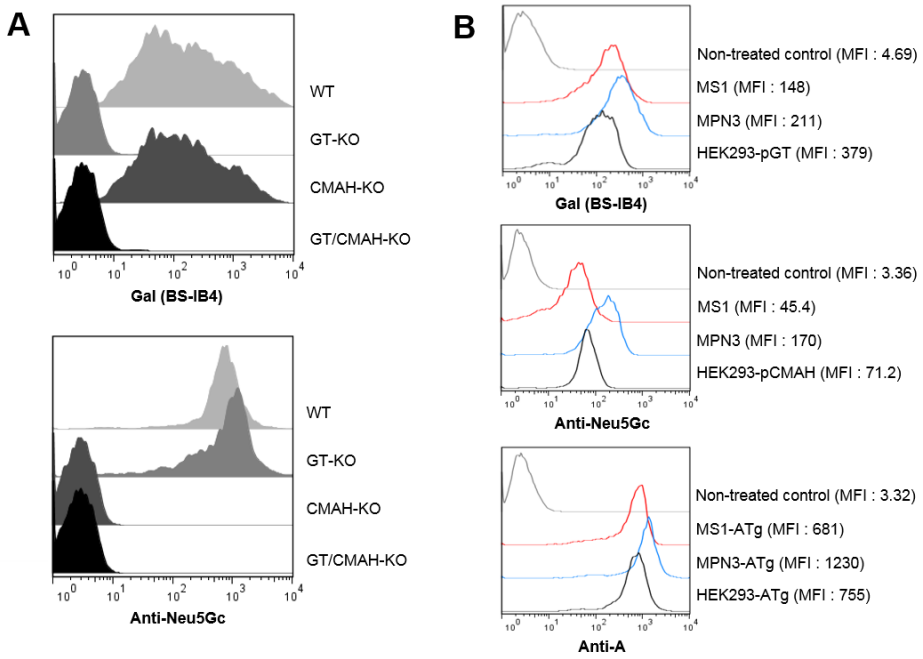

Figure 1. The expression of each carbohydrate antigen on indicated mice splenocytes and cell lines.

A-B) The spelenocytes from each mice (A) and indicated cell lines (B) were used for carbohydrate antigen staining and analyzed using flow cytometry. For α1,3Gal detection, the cells were incubated with the FITC-conjugated BS-IB4 lectin. For Neu5Gc detection, the cells were incubated with the chicken anti-Neu5Gc Ab, followed by the FITC-conjugated anti-chicken IgY Ab. For the detection of blood group A antigen, FITC-conjugated mouse anti-human blood group A Ab. MFI, mean fluorescence intensity.

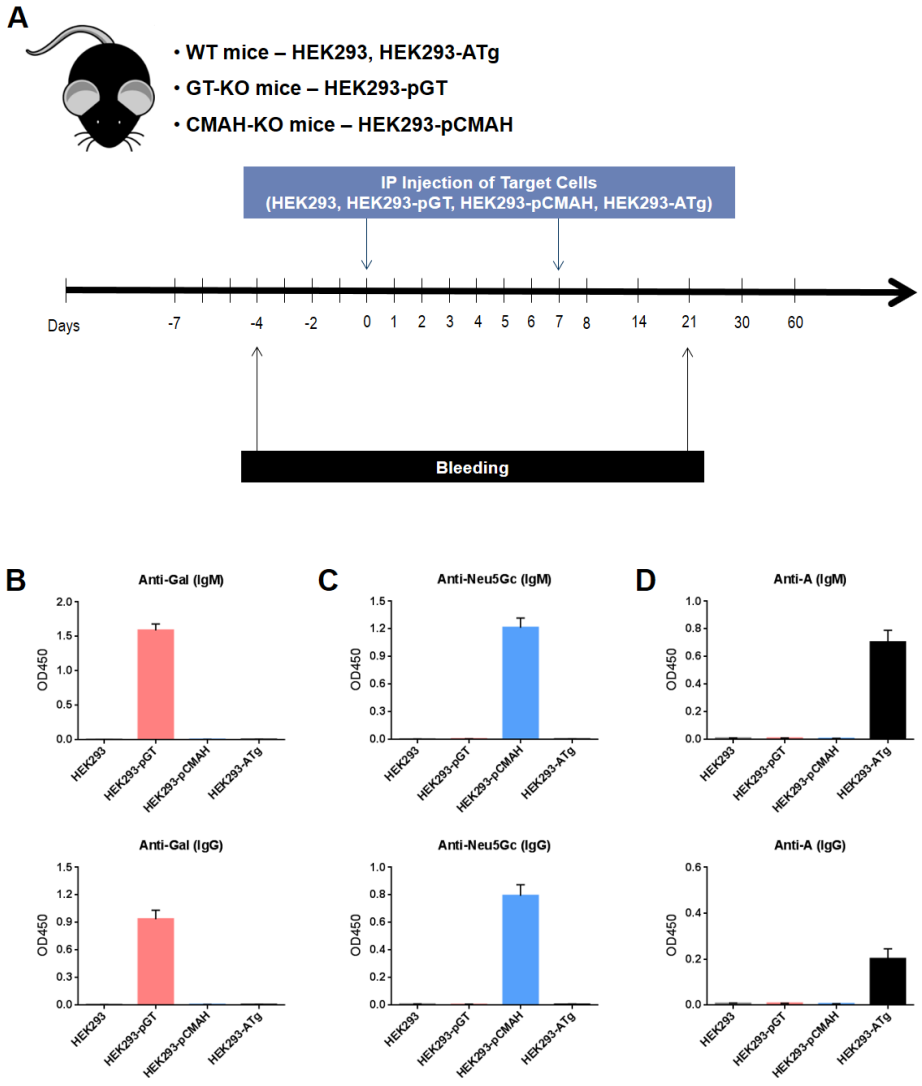

Figure 2. Induced antibodies production against target carbohydrate antigens and crossreactivity test.

A) Schematic diagram for the induced anti-carbohydrate antibodies production in mice. B-D) Using the serum samples from each indicated mouse (n=4, per group), the levels of IgM and IgG against α1,3Gal (B), Neu5Gc (C), or blood group A (D)

were analyzed by ELISA using α1,3Gal-PAA, Neu5Gcα-PAA, A-PAA, and control-PAA, respectively. For the detection of IgM or IgG bound to target antigens, HRP-conjugated goat anti-mouse IgM or IgG Ab, respectively. Bars represent mean absorbance values at OD450 ± SD for each group.

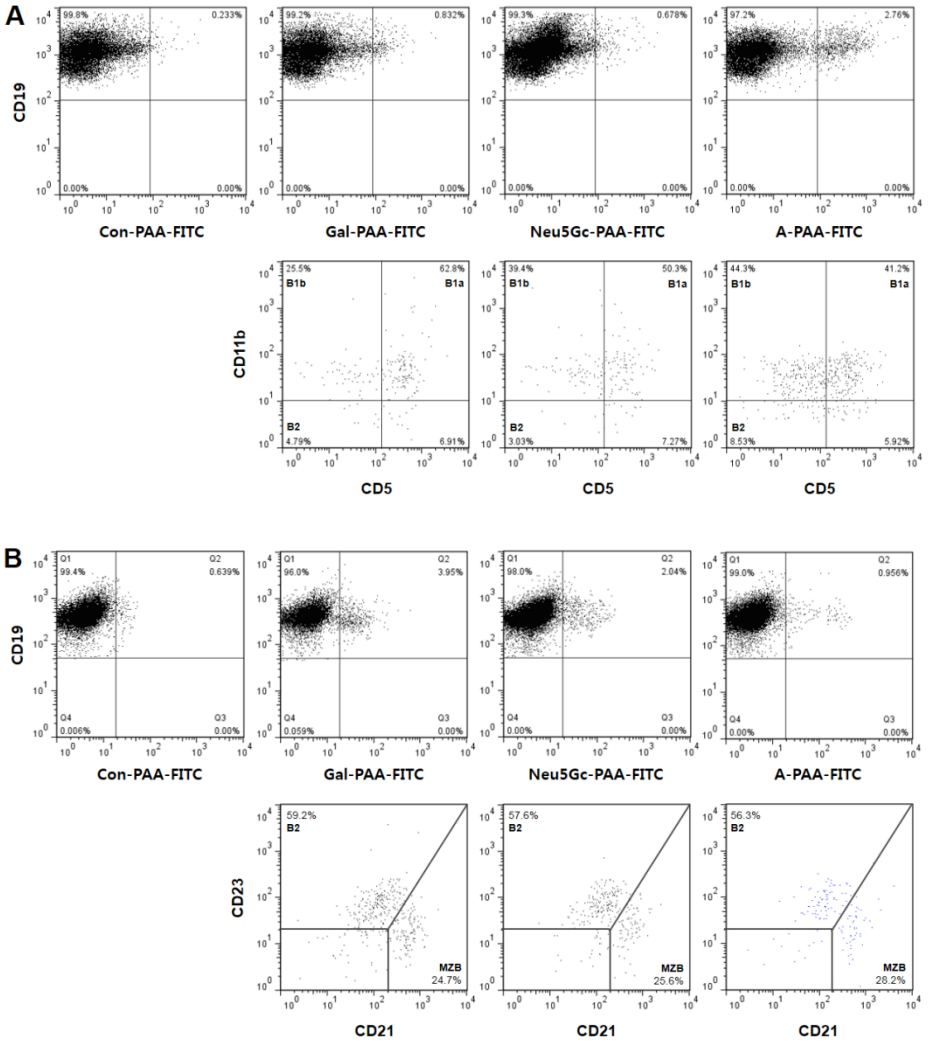

Figure 3. Subtype analysis of B cells responsible for antibodies production against each carbohydrate antigen.

A-B) Peritoneal exudate cells (A) or splenocytes (B) from each mouse were isolated and used to investigate which B cell subset react to indicated carbohydrate antigen. For detection of antigen binding to B cells, the cells were incubated with FITC-conjugated α1,3Gal-PAA, FITC-conjugated Neu5Gcα-PAA,

FITC-conjugated A-PAA, or FITC-conjugated Control-PAA, respectively. For subtype analysis of peritoneal B cells, the cells were stained with PE-conjugated rat anti-mouse CD19, APC-conjugated rat anti-mouse CD11b, and PE-Cy5-conjugated rat anti-mouse CD5. For subtype analysis of splenic B cells, the cells were stained with PE-conjugated rat anti-mouse CD19, AF647-conjugated rat anti-mouse CD23, and PerCP-Cy5.5-conjugated rat anti-mouse CD21/CD35.

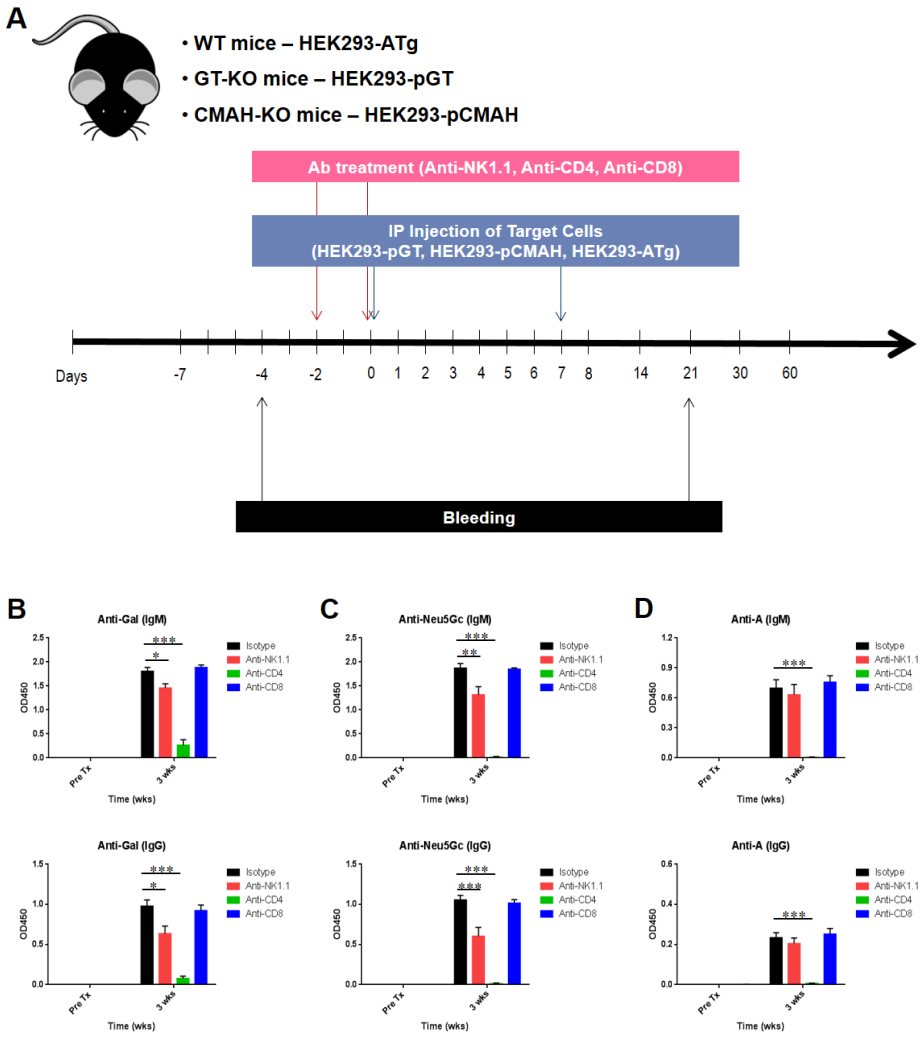

Figure 4. The effect of specific T cell depletion on induced anti-carbohydrate antibodies production in mice.

A) Schematic diagram for analyzing T cell-dependency in induced antibodies production against each carbohydrate antigen. B-D) Using each serum sample from four independent mice per group, the levels of IgM and IgG against α1,3Gal (B), Neu5Gc (C), or blood group A (D) were analyzed by ELISA using α1,3Gal-

PAA, Neu5Gcα-PAA, A-PAA, and control-PAA, respectively. For the detection of IgM or IgG bound to target antigens, HRP-conjugated goat anti-mouse IgM or IgG Ab, respectively. Bars represent mean absorbance values at OD450 ± SD for each group. For statistical analysis, one-way ANOVA with multiple comparison was used to compare results among groups.

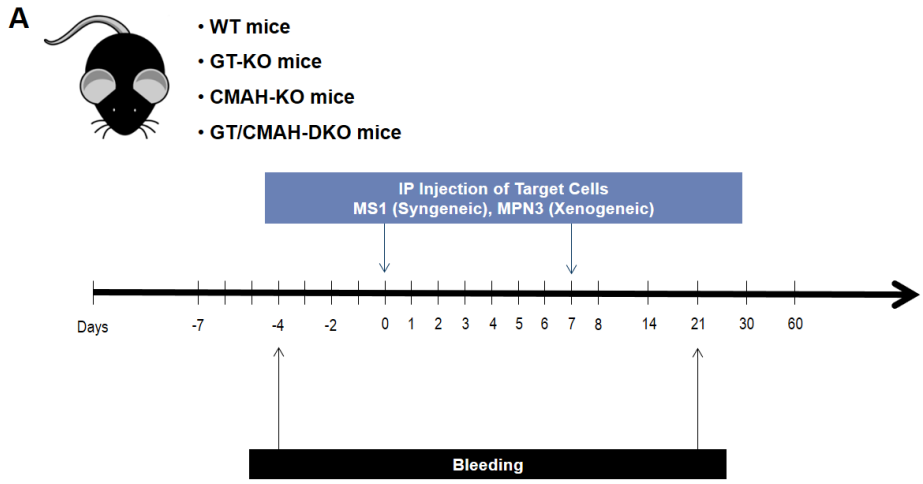
A
• WT mice
• GT-KO mice
• CMAH-KO mice
• GT/CMAH-DKO mice
IP Injection of Target Cells
MS1 (Syngeneic), MPN3 (Xenogeneic)
Days
-7
-4
-2
0
1
2
3
4
5
6
7
8
14
21
30
60
Bleeding

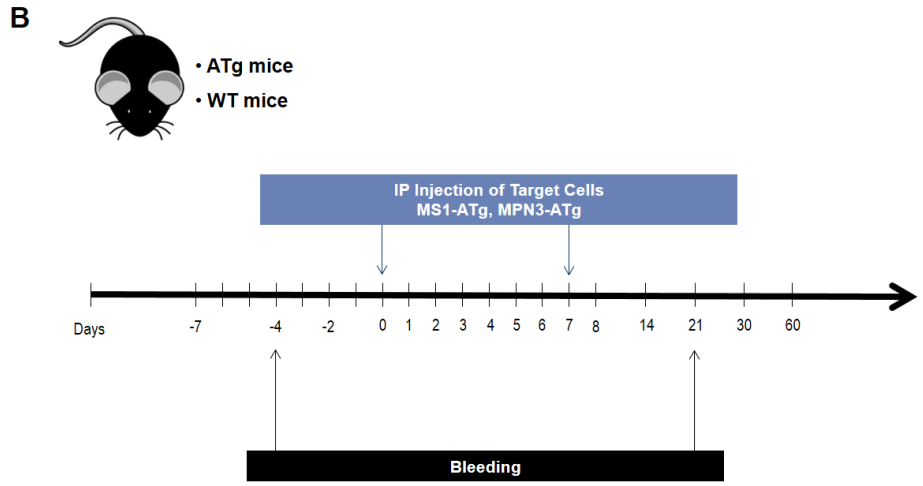
B
• ATg mice
• WT mice
IP Injection of Target Cells
MS1-ATg, MPN3-ATg
Days
-7
-4
-2
0
1
2
3
4
5
6
7
8
14
21
30
60
Bleeding

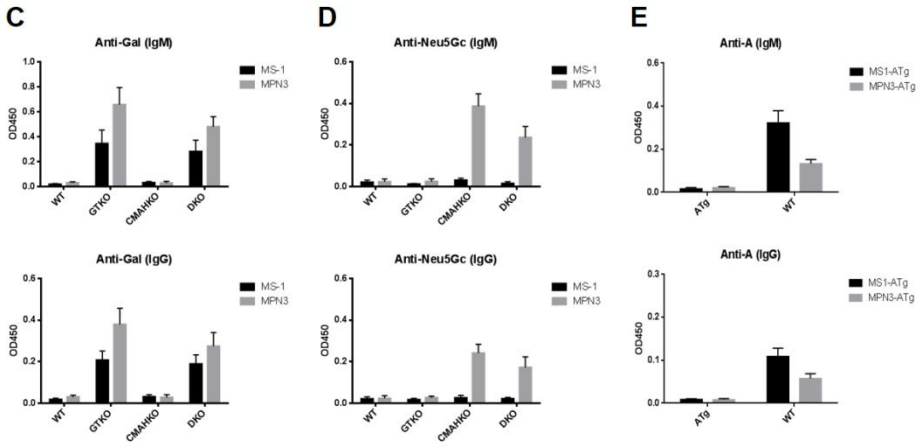
C
Anti-Gal (IgM)
Anti-Gal (IgG)
D
Anti-Neu5Gc (IgM)
Anti-Neu5Gc (IgG)
E
Anti-A (IgM)
Anti-A (IgG)
OD450
MS-1
MPN3
MS1-ATg
MPN3-ATg
WT
GTKO
CMAHKO
DKO
ATg

Figure 5. Induced antibodies production against each carbohydrate antigen by the stimulation with syngeneic or xenogeneic cells expressing target carbohydrate antigen.

A-B) Schematic diagrams to investigate the effect of the stimulation with syngeneic or xenogeneic cells expressing target carbohydrate antigen on induced antibodies production against each carbohydrate antigen, α1,3Gal, Neu5Gc (A), or blood group A (B) in mice. C-E) Using each serum sample from four independent mice per group, the levels of IgM and IgG against α1,3Gal (C), Neu5Gc (D), or blood group A (E) were analyzed by ELISA using α1,3Gal-PAA, Neu5Gcα-PAA, A-PAA, and control-PAA, respectively. For the detection of IgM or IgG, HRP-conjugated goat anti-mouse IgM or IgG Ab, respectively. Bars represent mean absorbance values at OD450 ± SD for each group.

Discussion

Unlike anti-protein antibody, which recognize a certain peptide region as an epitope, little is known about the mechanism for antibody binding to carbohydrate antigens. In this study, I provoked the production of induced antibody against three independent carbohydrate antigens, α1,3Gal, Neu5Gc, and blood group A antigen, in specific mice model using immunization protocol with some mammalian cells expressing each carbohydrate antigen. In order to investigate the specificity of the produced anti-carbohydrate antibodies, I checked whether the antibodies against a certain carbohydrate antigen have crossreactivity to the other carbohydrate antigens used in this study. Serum samples from WT mice immunized with HEK293 or MPN3 had no antibody against the three indicated carbohydrate antigens. The induced antibodies against α1,3Gal, Neu5Gc, or blood group A antigen bound to a specific carbohydrate antigen without any crossreactivity to the others.

In flow cytometric analysis of B cell subtype which is reactive to the three indicated carbohydrate antigens in in vitro, I observed that splenic B2 cells and MZ B cells mainly bound to α1,3Gal or Neu5Gc antigen. On the other hand, main population of blood group A-reactive B cells was peritoneal B1a and B1b cells. It is required to be explored furtherly that these B cell subtypes are actually involved in induced antibody production against these carbohydrate antigens and whether the antigen-specific germinal center are formed in these responses in mice model.

In terms of anti-peptide antibodies production, it is well known that peptide

antigens are presented to $CD4^+$ T cells via MHC class II molecules and the interaction between T cells and B cells develop germinal center formation to make affinity-maturated and isotype-switched antibody against target peptides [14]. Over the last decade, it is believed that carbohydrate antigens are T cell-independent antigens and anti-carbohydrate antibody are produced by B1 cells and MZ B cells without T cell help. It might be true that natural anti-carbohydrate antibody which are provoked by intestinal microbiome or pathogens can be produced without T cell help. However, it is unclear whether T cell help is required for the production of induced anti-carbohydrate antibody in certain glycan-incompatible transplantation situations. These data showed that treatment with anti-NK1.1 antibody partially inhibited the production of induced antibody against α1,3Gal and Neu5Gc antigens. In addition, $CD4^+$ T cell depletion dramatically blocked antibody production against three indicated carbohydrate antigens even though minimal anti-α1,3Gal antibodies were detected in serum samples from $CD4^+$ T cell-depleted GT-KO mice immunized with HEK293-pGT.

Interestingly, the minimal antibody production against α1,3Gal antigen was also observed despite the Pan T cells depletion by anti-CD3 antibody treatment in GT-KO mice. It is previously reported that immunization with pig peripheral blood mononuclear cells (PBMCs) resulted in a significant increase of anti-α1,3Gal antibodies in GT-KO mice, but this response was markedly blocked in GT and T cell receptor β chain-deficient (GT/TCRβ-KO) mice. However, immunization with pig PBMCs induced minimal antibody production against α1,3Gal antigen in GT/TCRβ-KO mice or GT-KO mice with additional treatment of anti-CD154 antibody to block T-B cell interaction [23]. These results

suggested that minimal but significant induced antibodies against α1,3Gal antigen can be produced without T cell help in GT-KO mice by the antigen stimulation.

Tazawa et al. reported that immunization with human blood group A-expressing red blood cells (A-RBCs) significantly provoked anti-A antibody production in WT mice. However, anti-A antibody production by immunization with A-RBCs was entirely blocked in athymic nude mice or CD1d-KO mice. In addition, this response was partially inhibited in Jα18-KO mice, but there was no difference in induced anti-A antibody production between WT mice and MHC class II-deficient (C2D) mice [24]. These results make us to think that induced antibody production against blood group A antigen is implicated in CD1d molecule and invariant natural killer T (iNKT) cells. However, a recent data showed that 60% of the diversity of the TCRα repertoire was actually lacking in Jα18-KO mice due to suppressed transcription of T cell receptor alpha joining (Traj) gene segments upstream of Traj18 [25]. In order to clarify that NKT cells are fundamental in induced anti-A antibody production in mice, I treated anti-NK1.1 antibody for the depletion of NKT cells in this system because B6 mice are well known strain to express NK1.1 on NKT cell surface despite the absence of NK1.1 in other common mouse strains [26, 27]. Contrary to my expectation, NKT cell depletion did not inhibit induced anti-A antibody production. Meanwhile, induced anti-A antibody production was absolutely suppressed by $CD4^+$ T cell depletion. These findings suggested that there are $NK1.1^-$ $CD4^+$ T cells which recognize glycolipid-borne blood group A antigen uploaded on CD1d molecules.

It is uncertain that when T cells response to glycopeptide on MHC molecules

or glycolipid on CD1d, T cell can recognize a certain carbohydrate portion and discriminate the difference. Avci et al. reported that in antigen presenting cells (APCs) a certain carbohydrate epitope can be preserved upon endolysosomal processing of glycoprotein and bind to MHC class II molecules to activate $CD4^+$ T cells. In this response, they showed that $CD4^+$ T cells recognized the carbohydrate epitope on MHC class II molecules [28]. In this study, after identifying $CD4^+$ T cells were crucial to induced antibody production against three indicated carbohydrate antigens in mice, I tried to investigate whether $CD4^+$ T cells recognized the indicated carbohydrate antigens using immunization with syngeneic cells or xenogeneic cells expressing each carbohydrate antigen. The significant production of induced antibody against α1,3Gal or blood group A antigen was observed despite immunization with syngeneic MS1 cells expressing each carbohydrate antigen. These results indicated that $CD4^+$ T cells can recognize α1,3Gal or blood group A antigen uploaded on certain presenting molecules on APCs. In the case of anti-Neu5Gc antibody production, interestingly, immunization with syngeneic MS1 cells did not provoke anti-Neu5Gc antibody in CMAH-KO mice even though MPN3 stimulation considerably increased anti-Neu5Gc antibody in the mice. I think that $CD4^+$ T cells cannot discriminate Neu5Gc antigen from N-acetylneuraminic acid (Neu5Ac) on presented glycopeptide, although sialylated antigen can be presented by APCs and the sialyation of antigen can influence T cells response to the antigen [29], and differences of peptide antigen are critical in induced anti-Neu5Gc antibody production.

In this study, I tested induced anti-carbohydrate antibody production in mice.

The induced antibodies against each carbohydrate antigens (α1,3Gal, Neu5Gc, or blood group A) are specific to target antigen and they do not have crossreactivity to the other antigens. I found that the production of induced antibodies against the carbohydrate antigens are all $CD4^+$ T cell-dependent responses and $NK1.1^+$ cells are partially involved the induced antibody production against α1,3Gal and Neu5Gc. The antigenic stimulation with syngeneic or xenogeneic cells expressing target carbohydrate can induce antibody production against α1,3Gal or blood group A, respectively. However, induced antibodies against Neu5Gc did not provoked by syngeneic MS1 stimulation even though the antibodies can be elicited by the stimulation with xenogeneic MPN3 in CMAH-KO mice.

References

1. Fong SW, Qaqundah BY, Taylor WF. Developmental patterns of ABO isoagglutinins in normal children correlated with the effects of age, sex, and maternal isoagglutinins. Transfusion. 1974;14(6):551-559.

2. West LJ, Pollock-Barziv SM, Dipchand AI, et al. ABO-incompatible heart transplantation in infants. The New England journal of medicine. 2001;344(11):793-800.

3. Taylor RE, Gregg CJ, Padler-Karavani V, et al. Novel mechanism for the generation of human xeno-autoantibodies against the nonhuman sialic acid N-glycolylneuraminic acid. The Journal of experimental medicine. 2010;207(8):1637-1646.

4. Porter KA. The effects of antibodies on human renal allografts. Transplantation proceedings. 1976;8(2):189-197.

5. Toma H. ABO-incompatible renal transplantation. The Urologic clinics of North America. 1994;21(2):299-310.

6. Cooper DK, Koren E, Oriol R. Oligosaccharides and discordant xenotransplantation. Immunological reviews. 1994;141:31-58.

7. Platt JL. A perspective on xenograft rejection and accommodation. Immunological reviews. 1994;141:127-149.

8. Alexandre GP, Squifflet JP, De Bruyere M, et al. Present experiences in a series of 26 ABO-incompatible living donor renal allografts. Transplantation

proceedings. 1987;19(6):4538-4542.

9. Tanabe K, Takahashi K, Sonda K, et al. Long-term results of ABO-incompatible living kidney transplantation: a single-center experience. Transplantation. 1998;65(2):224-228.

10. Kuwaki K, Tseng YL, Dor FJ, et al. Heart transplantation in baboons using alpha1,3-galactosyltransferase gene-knockout pigs as donors: initial experience. Nature medicine. 2005;11(1):29-31.

11. Chen G, Qian H, Starzl T, et al. Acute rejection is associated with antibodies to non-Gal antigens in baboons using Gal-knockout pig kidneys. Nature medicine. 2005;11(12):1295-1298.

12. Hardy RR, Hayakawa K. B cell development pathways. Annual review of immunology. 2001;19:595-621.

13. Shen P, Fillatreau S. Antibody-independent functions of B cells: a focus on cytokines. Nature reviews. Immunology. 2015;15(7):441-451.

14. Victora GD, Nussenzweig MC. Germinal centers. Annual review of immunology. 2012;30:429-457.

15. Wuttke NJ, Macardle PJ, Zola H. Blood group antibodies are made by CD5+ and by CD5- B cells. Immunology and cell biology. 1997;75(5):478-483.

16. Cerutti A, Cols M, Puga I. Marginal zone B cells: virtues of innate-like antibody-producing lymphocytes. Nature reviews. Immunology. 2013;13(2):118-132.

17. Vinuesa CG, Chang PP. Innate B cell helpers reveal novel types of antibody responses. Nature immunology. 2013;14(2):119-126.

18. Kim D, Kim JY, Koh HS, et al. Establishment and characterization of endothelial cell lines from the aorta of miniature pig for the study of xenotransplantation. Cell biology international. 2005;29(8):638-646.

19. Hurh S, Kang B, Choi I, Cho B, Lee EM, Kim H. Human antibody reactivity against xenogeneic N-glycolylneuraminic acid and galactose-alpha-1,3-galactose antigen. 2016;23(4):279-292.

20. Motyka B, Fisicaro N, Wang SI, et al. Antibody-Mediated Rejection in a Blood Group A-Transgenic Mouse Model of ABO-Incompatible Heart Transplantation. Transplantation. 2016;100(6):1228-1237.

21. Gock H, Murray-Segal L, Salvaris E, Cowan PJ, D'Apice AJ. Gal mismatch alone causes skin graft rejection in mice. Transplantation. 2002;74(5):637-645.

22. Hedlund M, Tangvoranuntakul P, Takematsu H, et al. N-glycolylneuraminic acid deficiency in mice: implications for human biology and evolution. Molecular and cellular biology. 2007;27(12):4340-4346.

23. Cretin N, Bracy J, Hanson K, Iacomini J. The role of T cell help in the production of antibodies specific for Gal alpha 1-3Gal. Journal of immunology (Baltimore, Md. : 1950). 2002;168(3):1479-1483.

24. Tazawa H, Irei T, Tanaka Y, Igarashi Y, Tashiro H, Ohdan H. Blockade of invariant TCR-CD1d interaction specifically inhibits antibody production against blood group A carbohydrates. Blood. 2013;122(15):2582-2590.

25. Bedel R, Matsuda JL, Brigl M, et al. Lower TCR repertoire diversity in Traj18-deficient mice. Nature immunology. 2012;13(8):705-706.

26. Smyth MJ, Crowe NY, Godfrey DI. NK cells and NKT cells collaborate in host protection from methylcholanthrene-induced fibrosarcoma. International immunology. 2001;13(4):459-463.

27. Stenstrom M, Skold M, Andersson A, Cardell SL. Natural killer T-cell populations in C57BL/6 and NK1.1 congenic BALB.NK mice-a novel thymic subset defined in BALB.NK mice. Immunology. 2005;114(3):336-345.

28. Avci FY, Li X, Tsuji M, Kasper DL. A mechanism for glycoconjugate vaccine activation of the adaptive immune system and its implications for vaccine design. Nature medicine. 2011;17(12):1602-1609.

29. Perdicchio M, Ilarregui JM, Verstege MI, et al. Sialic acid-modified antigens impose tolerance via inhibition of T-cell proliferation and de novo induction of regulatory T cells. Proceedings of the National Academy of Sciences of the United States of America. 2016;113(12):3329-3334.

국문 초록

장기이식은 말기의 장기부전 환자에게 가장 효과적인 치료 방법이지만, 공여장기의 부족으로 인해 치료가 제한적으로 이루어지고 있다. 동종 혈액형 부적합 장기이식 및 돼지의 장기를 이용한 이종 장기이식과 같은 글리칸 부적합 장기이식이 이러한 공여장기 부족 현상을 완화해줄 것으로 기대되고 있다. 그러나, 글리칸 부적합 장기이식의 성공을 위해서는 몇 가지 해결해야 할 문제들이 있고, 그 중에서도 공여자 혈관 내피의 글리칸 항원에 대한 항체매개성 면역반응의 조절이 필요하다.

첫째로, 인간과 돼지의 분자부적합성으로 인해 돼지의 혈관에 인간 항체의 경미한 결합에 의해서도 보체계 및 응고계 활성화가 유도될 수 있다. 분자부적합성으로 인한 이식 거부반응을 해결하기 위해서는 다양한 인간의 유전자를 발현하는 형질전환돼지의 개발이 필요하다. 그러나, 기존의 단일 형질전환돼지의 교배 또는 다수의 단일 시스트론성 벡터의 삽입으로 만들어진 다중형질전환 돼지의 경우는 목표 유전자의 발현이 고르지 않은 문제점이 있었다. 본 연구에서는 다양한 목표 유전자를 고르게 발현시키기 위해서 thosea asigna 바이러스 유래의 2A 펩티드 (T2A)를 활용한 다중 시스트론성 발현 시스템을 구축 및 평가하였다. T2A 발현 시스템을 이용하여 이종 장기이식에서 많이 사용되는 유전자들을 2 종씩 발현하는 벡터를 다수 제작하였고, 돼지의 섬유아세포에 유전자를 도입하여 각 유전자의

발현 양상을 분석한 결과 세포내 목표 발현 위치가 서로 다른 유전자 조합의 경우에도 문제없이 목표 발현 위치에 잘 발현됨을 확인하였다. 그리고 앞쪽에 위치한 유전자가 효과적으로 발현되는 경우에 뒤쪽에 위치한 유전자들도 효과적으로 발현됨을 확인할 수 있었다. 따라서, T2A 발현 시스템을 이용한다면 이종 장기이식을 위한 다중형질전환 돼지의 생산이 보다 용이할 것으로 기대된다.

둘째로, 돼지의 글리칸 항원에 대한 인간의 기존항체 결합으로 발생하는 체액성 면역반응의 조절이 필요하다. 초급성 거부반응을 일으키는 알파갈 항원이 적중된 돼지의 개발에도 불구하고, 비알파갈 항원에 대한 항체의 결합으로 인해 급성 체액성 이종이식편 거부반응이 유도된다. 다양한 비알파갈 항원 중에서도 N-글리콜릴 뉴라민산이 인간에서 강한 항원성을 가질 것으로 생각되고 있다. N-글리콜릴 뉴라민산에 대한 인간의 기존항체 반응을 분석하기 위해 N-글리콜릴 뉴라민산을 발현하는 HEK293 세포주를 구축하였고, 기존의 잘 알려진 알파갈 항원을 발현하는 HEK293 세포주와 비교하여 항원성을 분석하였다. 100 명의 인간 혈청을 각각 반응시켜본 결과, 알파갈 항원에는 IgM, IgG 타입의 항체가 모두 결합한 반면, N-글리콜릴 뉴라민산에는 주로 IgG 타입의 항체가 결합하였다. 대부분의 혈청 항체가 알파갈에 강하게 반응한 반면, N-글리콜릴 뉴라민산에 대한 반응은 개체 별로 반응성이 다양하였고, 일부 혈청과의 반응에서는 강한 세포독성이 유도되었다. 그리고, N-

글리콜릴 뉴라민산에 대한 인간 혈청의 반응정도와 알파갈 적중 돼지 혈관내피세포에 대한 인간 혈청의 반응정도 사이에는 양의 연관성이 있음을 확인하였고, 이는 알파갈 적중 돼지에서 N-글리콜릴 뉴라민산이 중요한 잔여 항원임을 보여주는 결과이다. 따라서, N-글리콜릴 뉴라민산을 합성하는 CMAH 유전자를 추가적으로 적중시킨 돼지의 개발을 통해 보다 많은 사람에게 돼지 장기를 도입할 수 있을 것으로 기대된다.

셋째로, 알파갈 적중돼지 및 항체 탈감작 치료법을 통해 초급성 거부반응을 극복하더라도 이식 후에 새롭게 형성되는 유도항체에 의한 급성 및 만성 항체매개성 거부반응은 또 하나의 문제이다. 이러한 글리칸 항원에 대한 유도항체의 생성에 있어서, 어떠한 B-세포 아형이 특정 글리칸 항원에 반응하는지, 이 반응은 T-세포 의존성 반응인지, T-세포는 항원제시분자 표면의 글리칸 항원을 인지할 수 있는지 등에 관해서는 잘 알려져 있지 않아 그 기전에 대한 연구가 필요하다. 본 연구에서는 특정 글리칸 항원이 적중된 마우스, 특정 글리칸 항원을 발현하는 세포주 등을 이용하여 특정 글리칸 항원 특이적인 유도항체 생성 마우스 모델을 구축하였고, 이를 통해 알파갈, N-글리콜릴 뉴라민산, 혈액형 A 항원에 대한 유도항체 생성 기전을 분석하였다. 각 글리칸 항원에 대한 유도항체는 항원 특이성을 갖는 항체임을 확인할 수 있었다. 그리고, 각 항원에 대한 유도항체 생성 기전은 항원 별로 다소 차이가 있었다. 흥미롭게도, 마우스 모델을

이용한 항-글리칸 유도항체 생성에서 CD4 양성 T-세포를 제거한 경우 항체의 생성이 현격하게 감소되었다. 따라서, CD4 양성 T-세포 조절이 인간이나 영장류에서도 항-글리칸 유도항체의 생성을 억제하는가에 대한 후속 연구가 필요할 것이다.

주요어: 글리칸 항원, 기존 항체, 유도 항체, 채액성 면역반응, ABO 혈액형 부적합 장기이식, 이종 장기이식, 다중 시스트론성 발현 시스템

학 번: 2011-31149